HHS Public Access

Author manuscript

Cell Rep. Author manuscript; available in PMC 2025 January 28.

Published in final edited form as:

Cell Rep. 2024 November 26; 43(11): 114925. doi:10.1016/j.celrep.2024.114925.

Muscle inflammation is regulated by NF-κB from multiple cells to control distinct states of wasting in cancer cachexia

Benjamin R. Pryce[1], **Alexander Oles**[1], **Erin E. Talbert**[1,2], **Martin J. Romeo**[3,4], **Silvia Vaena**[3], **Sudarshana Sharma**[4], **Victoria Spadafora**[1], **Lauren Tolliver**[1], **David A. Mahvi**[5], **Katherine A. Morgan**[5], **William P. Lancaster**[5], **Eryn Beal**[5], **Natlie Koren**[5], **Bailey Watts**[5], **Morgan Overstreet**[5], **Stefano Berto**[6], **Suganya Subramanian**[6], **Kubra Calisir**[4], **Anna Crawford**[3,7], **Brian Neelon**[3,7], **Michael C. Ostrowski**[3,4], **Teresa A. Zimmers**[8], **James G. Tidball**[9], **David J. Wang**[1], **Denis C. Guttridge**[1,3,10,*]

[1]Department of Pediatrics, Darby Children's Research Institute, Medical University of South Carolina, Charleston, SC 29425, USA

[2]Department of Health and Human Physiology, and the Holden Comprehensive Cancer Center, University of Iowa, Iowa City, IA 52242, USA

[3]Hollings Cancer Center, Medical University of South Carolina, Charleston, SC 29425, USA

[4]Department of Biochemistry and Molecular Biology, Medical University of South Carolina, Charleston, SC 29425, USA

[5]Department of Surgery, Medical University of South Carolina, Charleston, SC 29403, USA

[6]Department of Neuroscience, Medical University of South Carolina, Charleston, SC 29425, USA

[7]Department of Public Health Sciences, Medical University of South Carolina, Charleston, SC 29425, USA

[8]Department of Cell, Developmental, and Cancer Biology, Knight Cancer Institute, Portland, Oregon Health Science University, Portland, OR 97239, USA

[9]Department of Integrative Biology and Physiology, University of California, Los Angeles, Los Angeles, CA 90095, USA

[10]Lead contact

*Correspondence: guttridg@musc.edu.

AUTHOR CONTRIBUTIONS

B.R.P., E.E.T., D.J.W., M.C.O., T.A.Z., J.G.T., and D.C.G. conceptualized, designed, and performed the experiments. B.R.P., E.E.T., D.J.W., M.J.R., S.V., V.S., L.T., and D.C.G. were involved in the methodology. D.A.M., K.A.M., W.P.L., E.B., M.O., B.R.P., E.E.T., and D.C.G. were involved in obtaining patient materials. A.O., S. Sharma, S. Subramanian, S.B., K.C., B.R.P., B.N., A.C., and D.J.W. performed the bioinformatics and statistical analysis. B.R.P., V.S., and D.J.W. validated the data. B.R.P. and D.C.G. planned and outlined the manuscript and wrote the original draft, while editing was performed by all the authors. B.R.P., D.J.W., and D.C.G. led the supervision and D.C.G. the project administration. B.R.P., E.E.T., D.J.W., D.C.G., T.A.Z., and M.C.O. were involved in acquiring the funding to support the work.

DECLARATION OF INTERESTS

T.A.Z. is a scientific advisory board member of Emmyon, Inc. and PeleOS, LLC.

SUPPLEMENTAL INFORMATION

Supplemental information can be found online at https://doi.org/10.1016/j.celrep.2024.114925.

SUMMARY

Although cancer cachexia is classically characterized as a systemic inflammatory disorder, emerging evidence indicates that weight loss also associates with local tissue inflammation. We queried the regulation of this inflammation and its causality to cachexia by exploring skeletal muscle, whose atrophy strongly associates with poor outcomes. Using multiple mouse models and patient samples, we show that cachectic muscle is marked by enhanced innate immunity. Nuclear factor κB (NF-κB) activity in multiple cells, including satellite cells, myofibers, and fibro-adipogenic progenitors, promotes macrophage expansion equally derived from infiltrating monocytes and resident cells. Moreover, NF-κB-activated cells and macrophages undergo crosstalk; NF-κB$^+$ cells recruit macrophages to inhibit regeneration and promote atrophy but, interestingly, also protect myofibers, while macrophages stimulate NF-κB$^+$ cells to sustain an inflammatory feedforward loop. Together, we propose that NF-κB functions in multiple cells in the muscle microenvironment to stimulate macrophages that both promote and protect against muscle wasting in cancer.

In brief

We demonstrate that NF-κB functions in multiple cells in skeletal muscle to expand macrophages during cancer cachexia, deriving from infiltrating monocytes and resident cells. Macrophages contribute to muscle wasting and preservation of myofibers. They also crosstalk with muscle stem cells, myofibers, and fibro-adipogenic progenitors to sustain NF-κB activity and inflammation.

Graphical abstract

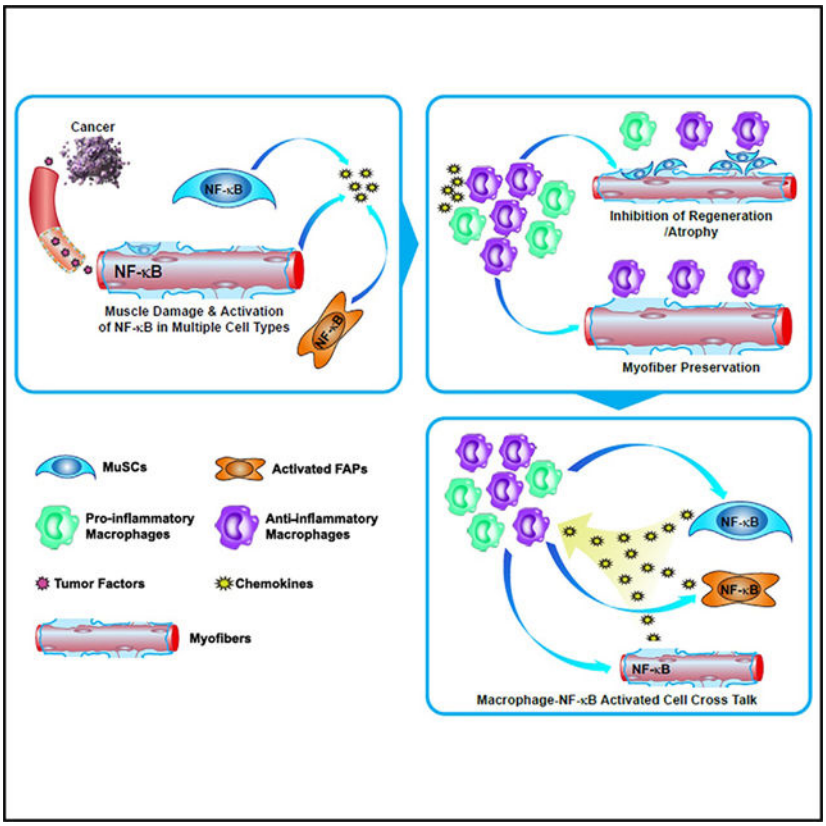

INTRODUCTION

Cancer cachexia is a debilitating syndrome characterized by unintentional weight loss due to the depletion of adipose and skeletal muscle mass.[1] Cachexia occurs in at least half of all patients with cancer and is estimated to account for greater than 20% of all cancer deaths.[2] In pancreatic ductal adenocarcinoma (PDAC), which has a 5-year survival rate of 13%,[3] the cachexia burden can be as high as 80%, associating with poor outcomes.[4,5] Mitigating cachexia has the potential to increase survival and the quality of life of patients with cancer. However, other than one approved product in Japan,[6] no effective treatment for cachexia currently exists, underscoring the need to increase our understanding of this disease.

Although cachexia affects multiple organs, it is the wasting of muscle that contributes most to the loss of body weight and underlying weakness, fatigue, and frailty. Significant advances have been made in comprehending the mechanisms of muscle wasting. Tumor and host factors signal to muscle myofibers to activate the ATP-dependent ubiquitin proteasome and lysosomal autophagy systems,[7] which in turn mediate muscle protein breakdown and reduced muscle mass.[8] Furthermore, tumor-associated reductions in insulin growth factor signaling in myofibers lowers Akt/mTOR activity and inhibits protein synthesis, leading to exacerbated muscle loss.[9]

Aside from these signaling cues that act intrinsic to the muscle fiber, tumor factors also regulate muscle wasting by signaling outside the myofiber, specifically on muscle stem

cells (MuSCs), to impair their differentiation in response to tumor-induced injury.[10] This exacerbates muscle atrophy due to the proteolytic pathways acting within the myofiber.[10] Such events predict that muscle atrophy in cancer occurs by a combination of protein breakdown, inhibition of protein synthesis, and impairment of muscle regeneration.[10]

While the precise tumor-associated factors that regulate myofiber atrophy and impair muscle regeneration remain to be fully identified, it has been assumed that such factors associate with systemic inflammation, characteristic of cancer cachexia.[2] In animal studies, circulating levels of cytokines tumor necrosis factor (TNF), interleukin (IL)-6, IL-1β, and interferon (IFN)-γ are elevated in cachexia and contribute to muscle catabolism and impaired muscle regeneration *in vitro* and *in vivo*.[11] However, whether similar levels of cytokines associate with cachectic patients with cancer is not as clear.[12–15] Aside from their systemic effects, we considered the possibility that inflammatory factors also promote muscle wasting by functioning at a more local level, within the tissue microenvironment. This notion is consistent with past findings in the Walker 256 model of cancer cachexia, where adipose loss associated with infiltrating macrophages,[16] or in a transplant model of PDAC where weight loss resulted from increases in neutrophils in the hippocampus.[17] A separate study with autopsy muscles from patients with PDAC showed elevated macrophages.[18] Such evidence supports that cancer cachexia associates with local tissue inflammation. However, what underlying mechanisms regulate muscle inflammation in cancer, and what its causality is to cachexia, remain largely unknown.

In this study, we find that muscle inflammation indeed associates with tumor-induced cachexia and reveal that local expression of inflammatory factors and recruitment of immune cells are largely under the control of nuclear factor κB (NF-κB). We further show that NF-κB orchestrates this local inflammatory environment by functioning in multiple cellular compartments and by participating in a signaling crosstalk with macrophages to regulate various activities relevant to muscle loss in cancer.

RESULTS

Muscle wasting in cancer cachexia associates with the accumulation of innate immune cells

Since muscle regeneration in acute and chronic injury is dependent on an immune response,[19] and muscle injury has been described in cancer cachexia,[10,20] we speculated that local inflammation existed in cachectic muscle. Thus, inflammatory cytokines TNF, IL-1β, and IL-6 were analyzed in hindlimb muscles from three mouse models of cancer cachexia, Colon-26 (C-26), Lewis lung carcinoma (LLC), and a more recently described genetic model of PDAC (KPP).[21] A general elevation of these cytokines was observed (Figure S1A). When this analysis was expanded using a panel of inflammatory genes, muscles from C-26, LLC, and to a lesser degree KPP displayed clusters of elevated expression of inflammatory genes compared to control (Figure 1A). These findings demonstrate that muscle inflammation associates with cancer cachexia.

Since cytokines regulate accumulation of immune cells during muscle injury,[19] flow cytometry was used to determine the immune cell composition of cachectic muscle (Figure

S1B and gating strategy in Figure S1C). Increases in the total number of $CD45^+$ cells were observed in the C26 and LLC models (Figure S2A). Myeloid cells, as a percentage of $CD45^+$ cells, were elevated in cachectic muscle from LLC and KPP models, reflecting increases in macrophages, neutrophils, and to a lesser degree eosinophils (Figure 1B). A similar trend occurred with total macrophages, neutrophils, and eosinophils in C-26, LLC, and KPP mice (Figure S2A). In contrast, lymphoid cells were elevated in muscles from C-26 tumor mice but reduced in LLC and KPP mice (Figure 1C). This regulation was reflected in $CD4^+$ T cells and T regulatory cells (Tregs). Similar trends occurred in $CD4^+$, $CD8^+$, Tregs, and natural killer (NK) cells (Figure S2A). Immunohistochemical staining with CD11b confirmed the increase in myeloid cells in C-26, LLC, and KPP muscles (Figures S2B and S2C). Although CD11b is also expressed in lymphoid cells,[22] little was detected on $CD4^+$ or $CD8^+$ T cells in muscle, and <2% was expressed on NK cells (Figure S1B and S1C; denoted by $CD161^+$, $CD11b^+$ staining), suggesting that, in skeletal muscle, CD11b is preferentially expressed in myeloid cells. F4/80 staining confirmed that increases in myeloid cells in cachectic muscles were representative of macrophages (Figure S2D).

To examine the relationship to patients, muscle biopsies from patients with PDAC with or without cachexia were examined. Results showed that IL-1β and IL-6 were significantly increased in muscles from patients with cachexia (Figure S2E). Muscle sections also exhibited a significant increase in myeloid cells in muscles from patients with cachexia compared to patients that were weight stable and controls (Figures 1D, 1E, and S2F). Cumulatively, these results show that cancer cachexia associates with local muscle inflammation, predominantly associating with innate immune cells.

Muscle inflammation in cancer cachexia is regulated by NF-κB from multiple cell types

Previously, we found that MuSCs were activated in cachectic muscle but were unable to complete differentiation due to a persistent NF-κB signal.[10] As NF-κB also stimulates the expression of inflammatory genes in MuSCs[23] and blocks their differentiation to contribute to muscle atrophy,[10] we postulated that NF-κB functions in these MuSCs during cachexia to regulate local muscle inflammation. To test this, we deleted NF-κB by conditionally ablating IKKβ kinase, which controls NF-κB activity, using *Pax7-Cre^{ER}*; *IKKβ $^{fl/fl}$* mice.[10] Although total hindlimb muscle failed to detect differences in expression of *TNF*, *IL-1β*, and *IL-6* cytokines between LLC tumor-bearing *Pax7-Cre^{ER}*; *IKKβ $^{fl/fl}$* mice and control (Figure 2A), a striking reduction in cytokines was seen when this analysis was repeated with mononuclear cells enriched for MuSCs (Figure 2B). This supported the conclusion that NF-κB regulates inflammation from MuSCs in cachectic muscle. To determine the extent of this regulation, we performed RNA sequencing (RNA-seq) from the same population of mononuclear cells described above from *Pax7-Cre^{ER}*; *IKKβ $^{fl/fl}$* muscles. In differentially expressed genes with a fold change greater than 2 ($p < 0.05$), 223 genes were downregulated, and 56 genes were upregulated in the absence of NF-κB (Figure 2C), revealing that NF-κB acts primarily as a transcriptional activator in the setting of cachexia. Additionally, gene ontology showed that the top classes of genes regulated by NF-κB from MuSCs associated with immune responses (Figure 2D). These included *chemokines (C-C motif) ligand 2* (*CCL2*), also referred to as *monocyte chemoattractant protein 1* (*MCP-1*); *(C-X-C motif) ligand 1* (*CXCL1*), and *(C-X-C motif) ligand 2* (*CXCL2*). We confirmed

that these chemokines were generally elevated in hindlimb muscles from C-26, LLC, and KPP mice (Figure S3A). Similar to inflammatory cytokines, *CCL2*, *CXCL1*, and *CXCL2* expression levels did not change between total *Pax7-Cre^{ER}*; *IKKβ $^{fl/fl}$* and *IKKβ $^{fl/fl}$* muscles (Figure S3B), whereas chemokines were strongly repressed when analyzed from mononuclear populations (Figure 2E). In addition, staining with CD11b and flow cytometry using F4/80 showed that macrophages were significantly reduced in *Pax7-Cre^{ER}*; *IKKβ $^{fl/fl}$* muscles from LLC-bearing mice compared to control (Figures 2F and 2G, and S3C). These results suggest that NF-κB functions in MuSCs as a regulator of muscle inflammation during cancer cachexia.

Given that NF-κB regulates inflammatory signals from myofibers in a mouse model of muscular dystrophy,[24] we asked whether myofibers are also involved in regulating muscle inflammation in cachexia. Examination of inflammatory genes showed significant reductions in *IL-1β*, *IL-6*, and *CCL2* in *HSA-Cre^{ER}*; *IKKβ $^{fl/fl}$* compared to *IKKβ $^{fl/fl}$* myofibers (Figure 2H), which corresponded to a similar reduction in macrophages (Figures 2I, 2J, and S3D). Taken together, our data suggest that macrophage accumulation in cachectic muscle is NF-κB dependent, and this dependency derives from a signaling activity localized to both MuSCs and myofibers.

Recent scRNA-seq results recognize fibro-adipogenic progenitors (FAPs) as one of the predominant mononuclear cell populations in resting skeletal muscle, and, during muscle injury, FAPs expand and transition to an activated phase, characterized by the expression of inflammatory genes.[25] We asked whether a similar phase of activation occurs in FAPs in cachectic muscle. Thus, we performed scRNA-seq on CD45^{-} cell fractions collected from muscles of C-26, KPP, and patients. We utilized uniform manifold approximation and projection (UMAP) to visualize individual transcriptomes of all CD45^{-} cells in the unified dataset, and unsupervised shared nearest-neighbor clustering separated cells into expected cellular subtypes in C-26 muscle samples. In C-26 muscles, segregation of populations compared to control revealed striking differences among FAPs (Figure S3E). Furthermore, graph-based clustering of FAPs revealed 10 distinct subpopulations, with some being exclusively restricted to either control or C-26 muscles (Figures 3A and 3B). *CCL2*, *CCL7*, and *CXCL1* were enriched in clusters 0 and 1 in cachectic muscle (Figure 3C), similar to their elevation in FAPs residing in injured muscle.[25] A parallel analysis performed in KPP mice showed an analogous number of cell clusters and proportions, comparable to C-26 muscles (Figure S3F). The subcluster of FAPs revealed 13 distinct populations between KPP and control muscles (Figures 3D and 3E), and similar increases in inflammatory genes from FAPs in KPP muscles associated with selected clusters (Figure 3F). To assess the significance of our findings, we performed scRNA-seq on CD45^{-} cells isolated from muscles of a control, wild-type (WT) stable, and cachectic patients with PDAC; the latter two were collapsed into one sample due to low cell recovery. Segregation of populations compared to a control patient showed fewer differences among FAPs as seen with the C-26 and KPP models (Figure S3G). However, clustering of FAPs identified eight distinct populations that segregated between patients and revealed subpopulations that were unique to control and patients with PDAC (Figures 3G and 3H). Although PDAC patients with cachexia exhibit even less inflammation compared to mouse models,[13] activated FAP

populations in muscles from patients with PDAC remained apparent, as shown by expression of the inflammatory chemokine *CXCL14*, enriched in clusters 0, 4, and 6 (Figure 3I).

From these results, we speculated that FAPs contributed to an inflammatory environment in cancer cachexia and, further, that NF-κB was involved in regulating this activity. Staining with the activated form of the p65 subunit showed that NF-κB co-localized to platelet-derived growth factor receptor-alpha-positive (PDGFRα$^+$) FAPs, and this signal increased in C-26 muscles, as well as in patients with PDAC and cachexia (Figures 3J and 3K). We next examined whether this NF-κB activity contributed to inflammation in cachectic muscle. Deletion of IKKβ from FAPs using *PDGFRα-Cre^{ER}*; *IKKβ$^{fl/fl}$* mice caused a reduction of macrophages in LLC tumor-bearing mice compared to control, which correlated with significant decreases in whole-muscle expression of cytokines and chemokine genes (Figures 3L and 3M and S3H). Although we had previously shown that deletion of IKKβ from MuSCs in LLC tumor-bearing mice rescued cachexia,[10] interestingly, here ablation of IKKβ from FAPs proved unsuccessful in achieving a similar rescue, as determined by outcome measures on body weight and muscle mass from two fast-type hindlimb muscles (Figures S3I and S3J). There was also no difference in tumor mass (Figure S3K). Nevertheless, when taken together, our data suggest that macrophage-mediated muscle inflammation in cancer cachexia is regulated by NF-κB signaling derived from multiple cell types in the muscle microenvironment.

Macrophages accumulate in cachectic muscle from circulating monocytes and expanding resident cells

Since recruitment of circulating monocytes into skeletal muscle is regulated by chemokines,[19] we next asked whether macrophage accumulation in cachectic muscle results from chemokines derived from different cellular compartments active in NF-κB. To test this, we first utilized CRISPR-Cas9 to knock down *CCL2*, *CXCL1*, and *CXCL2* from C2C12 myoblasts, which effectively reduced chemokine levels in conditioned media by 45%, 65%, and 63%, respectively (Figure 4A). Media from these myoblasts significantly reduced macrophage migration compared to control ($p < 0.05$; Figures S4A and 4B). This suggests that myoblasts secrete chemokines, likely under the control of NF-κB, to regulate recruitment of immune cells into muscle. We tested this *in vivo* by comparing both LLC *Pax7-Cre^{ER}*; *CCL2$^{fl/fl}$* and *HSA-Cre^{ER}*; *CCL2$^{fl/fl}$* mice to controls. In both lines, there was a significant reduction of macrophages in cachectic muscle (Figures 4C and 4D), suggesting that NF-κB acts in MuSCs and myofibers to secrete CCL2 and regulate macrophage accumulation.

To determine the origin of these macrophages, bone marrow cells from either CD45.2 or CD45.1 mice were transplanted into CD45.2 recipient C57BL/6 mice. After recovery, mice were injected with tumor cells and mononuclear cells were subsequently recovered from skeletal muscle following the development of cachexia. CD45.1$^+$ cells increased (Figure S4B), suggesting that a significant portion of immune cells in cachectic muscle derives from an infiltrating population. To verify our findings, bone marrow from *CCR2$^{-/-}$* mice, which lack the receptor required for CCL2 signaling, were transplanted into C57BL/6 recipient mice, and LLC cells were subsequently injected. Muscles from *CCR2$^{-/-}$*

transplants contained a significant reduction of macrophages compared to WT transplants (Figure 4E). This confirmed that circulating monocytes contribute to muscle inflammation in cancer in response to an NF-κB-mediated CCL2/CCR2 signal. However, using a separately designed antibody panel to detect tissue-resident macrophages (Figure S4C and gating strategy in Figure 4F), we estimated that, of the macrophages that accumulated in cachectic muscles from C-26, LLC, and KPP models, 56%, 69%, and 40% of these cells, respectively, originated from a tissue-resident pool (Figure 4G). Thus, both infiltrating and resident macrophages contribute nearly equally to total macrophages that accumulate in cachectic muscle. Significantly, deletion of NF-κB from MuSCs, myofibers, or FAPs, resulted in the reduced expansion of both infiltrating and resident macrophages (Figure 4H), suggesting that the total accumulation of macrophages in cachectic muscle is NF-κB dependent.

Macrophages both promote and protect against muscle wasting in cancer cachexia

Next, we addressed the causality of macrophage accumulation in cachectic muscle. To make this determination, macrophages were depleted from muscles of C-26 tumor mice with a liposome-encapsulated clodronate suspension (Figure 5A). Macrophage depletion was confirmed at endpoint by flow cytometry (Figure 5B). Although not significant, clodronate reduced tumor weight by approximately 20%, while body weight was unaffected (Figure 5B). Conversely, mass of the tibialis anterior (TA) and quadricep (QUAD) muscles were significantly increased by 30% and 33%, respectively ($p < 0.05$), while the gastrocnemius (GAST) muscle was modestly increased by 16% (Figure 5C). Concordantly, muscle cross-sectional area of the TA was increased (Figures 5D and 5E), which coincided with a decrease in expression of the E3 ubiquitin ligase atrophy markers, *MuRF1* (*Trim63*) and *Atrogin-1* (*MAFbx/Fbxo32*) (Figure 5F).[8] Such results imply that macrophages contribute to muscle wasting in cancer cachexia.

Since NF-κB promotes muscle wasting by blocking MuSC regeneration,[10] and since our current data indicate that NF-κB is required for macrophage accumulation in cachectic muscle (Figure 2), we asked whether macrophages promote muscle wasting by inhibiting MuSC regeneration. To this end, proliferating myoblasts were tracked with bromodeoxyuridine (BrdU) (Figure 5A). Results showed an appreciably higher number of sublaminar $BrdU^+$ myonuclei from clodronate compared to vehicle-treated tumor-bearing mice (2.7-fold; $p < 0.01$; Figures 5G and 5H). This shows that depleting macrophages increases the fusion of $BrdU^+$ myoblasts from the muscle interstitium into myofibers, resulting in a rescued regenerative program.

While these data support that macrophages promote muscle wasting in cachexia, several caveats were noted. First, since macrophages are required for tumor progression,[26] and their numbers are decreased in tumors from clodronate-treated mice (Figure S5A), we speculated that clodronate might indirectly affect tumor growth and thus alter cachexia.[27] Second, because clodronate suspensions are not absorbed in skeletal muscle, depletion is limited to macrophages derived from the circulation while the resident pool is spared. Our findings showed that resident cells modestly declined, likely resulting from an indirect effect (Figure S5B). Based on these caveats, we performed an additional experiment using CD11b-dipththeria toxin receptor (DTR) mice and administered diphtheria toxin (DTA)

intramuscularly, which should deplete both infiltrating and resident macrophages while having minimal impact on the tumor. Since DTR mice are in a C57BL/6 background, we utilized LLC tumor cells. DTA was subsequently injected into the TA (Figure 5I). Findings showed that DTA administration minimally impinged on tumor-associated macrophages while depleting both muscle-associated infiltrating and resident macrophages (Figures 5J, S5C, and S5D). In addition, DTA had no effect on tumor weight or body weight (Figure 5J) and, following BrdU injections, increased sublaminar $BrdU^+$ nuclei compared to control (1.46-fold; $p < 0.05$; Figures 5K and 5L), suggestive of enhanced regeneration. Interestingly, although no change in muscle mass was observed (Figure 5M), DTA treatment surprisingly reduced TA type IIA and IIB/X fiber sizes by 30% and 20%, respectively, while also increasing expression of *MuRF1* and *Atrogin-1* (Figures 5N–5P). Such findings suggested that, while the removal of macrophages rescued regeneration, their loss also promoted myofiber atrophy.

To verify our results, we repeated DTA experiments by backcrossing CD11b-DTR mice into a CD2F1 background and administered C-26 tumor cells (Figure S5E). Results were consistent with LLC mice, in that tumor weight and body mass were unchanged, regeneration was again significantly increased (2.1-fold, $p < 0.05$), but TA mass was decreased (33%, $p < 0.05$), along with reductions in fiber types IIA and IIB/X (35% and 23%, respectively; $p < 0.05$) (Figures S5F–S5K; $p < 0.05$). Taken together, these findings suggest that macrophages in cachectic muscle exhibit both pro- and anti-atrophy activities.

From the results above, we speculated that these distinct functions of macrophages in cachectic muscle are mediated through distinct cellular subtypes. Using flow cytometry to characterize macrophages accumulating in C-26 and KPP muscles (Figures S5L and gating strategy in Figure S5M), we observed that their increase almost entirely consisted of unpolarized and anti-inflammatory populations (Figures 6A and 6B). Smaller populations that remained represented pro-inflammatory and a mixture of macrophage subtypes. In KPP muscles, we further observed that anti-inflammatory macrophages accumulated early, by day 75 dpi (Figure 6B), a time when PDAC, but not muscle atrophy, has initiated.[21] Interestingly, this inflammation subsided over time, coinciding with muscle loss (Figure 6B).[21]

To test if pro-inflammatory or anti-inflammatory subtypes of macrophages have distinct functions in cachectic muscle, co-cultures with C2C12 myoblasts and bone marrow-derived macrophages were prepared. Under differentiation conditions, pro-inflammatory macrophages potently inhibited myoblast differentiation into myotubes, consistent with other reports (Figure 6C and 6D).[28] However, contrary to these same reports, we observed that anti-inflammatory macrophages also possessed myogenic inhibitory activity. When co-cultures were repeated with pre-differentiated myotubes, pro-inflammatory macrophages induced atrophy, decreasing myotube diameter by 42% ($p < 0.01$) (Figures 6E and 6F). In comparison, anti-inflammatory macrophages did not affect myotube diameter, suggesting that these cells possess a maintenance function. To test this, co-cultures were repeated with pre-differentiated myotubes. The addition of pro-inflammatory macrophages once again induced atrophy. However, further addition of anti-inflammatory macrophages at increasing concentrations that approached physiological ratios (Figure 6B; KPP, day 75) rescued myotube atrophy (Figure 6G). These findings suggest that distinct subtypes of macrophages

accumulate in cachectic muscle with distinct functions. Although pro-inflammatory and, to some degree, anti-inflammatory macrophages promote atrophy by inhibiting regeneration, anti-inflammatory macrophages function in maintaining myofiber size.

Phenotyping macrophages in cachectic muscle

We extended the characterization of macrophage subtypes in cancer cachexia by isolating mononuclear cells from C-26 and KPP muscles, enriched for $CD45^+$ fractions, and sequencing at the single-cell level. UMAPs visualized individual transcriptomes of all $CD45^+$ cells in the unified dataset. Unsupervised shared nearest-neighbor clustering separated cells into neutrophils, macrophages, T and B cells, NK cells, and dendritic cells, as well as some endothelial and stromal cells, which represented contaminating populations (Figures 7A and S6A). We then reclustered macrophages and identified a total of 12 distinct populations in C-26 muscles and 10 populations in KPP muscles that segregated between control and cachectic muscles (Figures 7B and S6B). In each dataset, macrophage subclusters were named based on genes with enriched expression in their respective clusters. For the C-26 dataset, the *S100a9* and *Lyve1* subclusters made up the largest percentages of macrophages (Figures S6B and S6C). In contrast, KPP muscle was enriched in a *Ccr2* subcluster as well as a unique *Lyve1* population (Figures 7B and 7C). Gene Ontology pathways revealed that both *Ccr2* and *S100a9* subclusters from KPP and C-26 models, respectively, were associated with ontologies related to bacterial infection and inflammation, suggesting that these populations are likely more pro-inflammatory in nature (Figures 7D and S6D). S100A9 acts as an endogenous ligand for pro-inflammatory receptors, Toll-like receptor 4 (TLR4), and receptor for advanced glycosylation end products (RAGE), and its elevated levels associate with inflammatory disease.[29,30] Conversely, *Lyve1* clusters were distinguished by genes associated with endocytosis (Figures 7E and S6E). *Lyve1* clusters from C-26 and KPP muscles expressed several established tissue-resident macrophage markers, Mef2c and Tcf4,[31] suggesting that these cells are resident in origin (Figures 7F and S6F). This population also expressed CD206, an anti-inflammatory marker used to also identify resident cells.[31]

To assess whether these macrophage phenotypes are recapitulated in human cachectic muscle, we performed similar scRNA-seq on patient samples. Unsupervised shared nearest-neighbor clustering between control and patients with PDAC separated cells into myeloid and lymphoid populations similar to those identified in C-26 and KPP muscles (Figure 7G). Re-clustering macrophages revealed similar distinct populations enriched in patients with PDAC compared to those identified in cachectic muscles from mouse models (Figures 7H and 7I). Patients with PDAC were also proportionally enriched in *S100A9* and *LYVE1*-expressing subclusters compared to the control patient (Figures 7H and 7I). Similar to C-26 and KPP muscles, the *S100A9* subcluster was linked with response to bacterial infection. The *LYVE1* subcluster exhibited gene ontologies associated with endocytosis (Figures 7J and 7K) and was enriched in the resident macrophage markers Mef2c and Tcf4 as well as CD206 (Figure 7L). Conversely, the *S100A9* cluster expressed pro-inflammatory genes, devoid of resident markers (Figure 7L). Taken together, these analyses indicate that *S100A9*-expressing populations are pro-inflammatory macrophages and originate from

infiltrating monocytes and *LYVE1* subclusters represent resident macrophages with potential anti-inflammatory properties.

Macrophages crosstalk with multiple cell types via NF-κB to regulate cachexia

Since we showed that NF-κB functioned in different cell types to recruit macrophages (Figures 2 and 3), we asked whether macrophages themselves were involved in crosstalk with these cells. We utilized similar co-cultures to those described above, with the exception that target cells contained an NF-κB luciferase reporter. With myoblasts, results showed that pro-inflammatory macrophages activated NF-κB, impressively, even when macrophages were seeded at a 1:50 macrophage-to-myoblast ratio (Figure S7A). Anti-inflammatory macrophages also activated NF-κB, albeit to lower levels. However, NF-κB was not activated when myoblasts were co-cultured with mouse embryonic fibroblasts (Figure S7B), suggesting a selective signaling interplay between myoblasts and macrophages. Further, results showed that pro-inflammatory and, to a lesser degree, anti-inflammatory macrophages were capable of stimulating myoblasts to express NF-κB-regulated chemokines *CCL2*, *CXCL1*, and *CXCL2* (Figure S7C). To inquire if soluble factors mediated this crosstalk, we investigated TNF and IL-1β, since both cytokines potently activate NF-κB. In co-culture assays, $TNF^{-/-}$ but not $IL\text{-}1\beta^{-/-}$ pro-inflammatory macrophages reduced NF-κB activity (Figure S7D and S7E). A similar reduction was not seen with $TNF^{-/-}$ or $IL\text{-}1\beta^{-/-}$ anti-inflammatory macrophages (Figure S7F and S7G). These results imply that pro-inflammatory and anti-inflammatory macrophages crosstalk with MuSCs in cachectic muscle, through NF-κB, via variable secreted factors. Using similar co-culture assays, we explored whether macrophages crosstalk with myotubes and FAPs. Results showed that both pro-inflammatory and anti-inflammatory macrophages activated NF-κB (Figures S7H and S7J) and chemokine expression in both cell types (Figures S7I and S7K). Such findings imply that activation of NF-κB in multiple cells in cachectic muscle participate in crosstalk with macrophages, likely leading to a feed-forward loop to sustain an inflammatory muscle environment.

DISCUSSION

This study was undertaken to gain insight on the underlying mechanisms of muscle wasting in cancer cachexia, specifically in relation to inflammation. Our results showed that cachectic muscle, similar to other findings in adipose, muscle, brain, and liver,[16,17,32–34] is associated with local inflammation. We investigated this inflammatory environment using multiple models of cancer cachexia and showed that this condition associates with elevated levels of cytokines and chemokines along with increases in innate immune cells, specifically macrophages. In contrast, cachectic muscles from LLC and KPP mice exhibited a reduction in lymphoid cells, which is consistent with what was reported in brain from a KPC transplant model of cachexia.[17] However, in C-26 mice, opposite results were observed, where cachectic muscle was instead associated with increases in lymphoid cells. These differences between models cannot yet be accounted for, but one possibility is the relation to strain, as LLC, KPP, and KPC models are in a C56BL/6 background, while the C-26 model is syngeneic to BALB/c mice. Further studies utilizing additional cachexia models and patient samples will be needed to better assess the regulation of lymphoid

cells in cachectic muscle in cancer. However, what seems clear is that peripheral tissue inflammation in cancer cachexia is marked by an increase in innate immunity, and, further, when referencing systemic inflammation as a hallmark feature of cancer cachexia, closer consideration should be given to how local tissue inflammation contributes to this systemic condition.

The triggers of tissue inflammation in cancer have not been well described. Previous studies have shown that activation of NF-κB in MuSCs and myofibers leads to muscle atrophy in various cachexia conditions[10,35,36] and our current results reveal that, in tumor mice, NF-κB functions in cachectic muscle as a major regulator of local inflammation through macrophage accumulation. We found that NF-κB directs this regulation from multiple cell types, including, but likely not limited to, MuSCs, myofibers, and FAPs. Furthermore, NF-κB-mediated accumulation of macrophages was regulated by CCL2. *In vitro* results showed that deletion of CCL2 from myoblasts reduced but did not completely eliminate macrophage migration, a finding that was mimicked by similar deletion of CXCL1 and CXCL2. It is likely that these chemokines, and others such as CCL7, contribute additively to the recruitment of macrophages in cachectic muscle.

Results from our study also provided detailed characteristics of macrophages. In KPP muscle, we appreciated that macrophages accumulate prior to atrophy, and this accumulation subsides during the active phase of muscle atrophy. We also found that expansion of these cells represents an almost equal contribution from circulating monocytes and tissue-resident cells. In addition, our single-cell data suggest that these cells polarize to an anti-inflammatory state. Eosinophils that accumulate in cachectic muscle might contribute to this regulation, as these cells secrete Th2-type cytokines IL-4 and IL-13, which function in macrophage polarization.[37] Consistent with previous reports in acute and chronic skeletal muscle injury models, our data reveal that macrophages are heterogeneous in cachectic muscle, consisting of multiple populations and exhibiting pro- and anti-inflammatory profiles.[25,38,39]

Functionally, we discovered that these macrophages likely act in diverse ways in cachexia. Removal of macrophages from LLC and C-26 muscles increased myoblast fusion, suggesting that these cells function in cachexia by inhibiting muscle regeneration to promote atrophy. Based on our current and published findings[10,40] we envision that this occurs through the activation of NF-κB in myoblasts to inhibit myogenesis. For pro-inflammatory macrophages, activation of NF-κB might be regulated through secretion of TNF, whereas, for anti-inflammatory macrophages, NF-κB activation and the block on myogenesis are mediated through other factors (Figure S7). Likewise, macrophages might inhibit muscle regeneration and promote atrophy through NF-κB crosstalk in myoblasts to maintain Pax7 expression and block differentiation, as previously described.[10] Thus, NF-κB secretes CCL2 to recruit macrophages, leading to further NF-κB activity to inhibit regeneration and promote atrophy. However, we also observed that depletion of macrophages reduced myofiber size, suggesting that macrophages in cachexia have an added role in maintaining muscle mass. We speculate that anti-inflammatory macrophages function to protect myofibers in a cachectic setting. This notion is consistent with KPP data (Figure 6), which showed that maximal muscle atrophy coincided with a reduction

from peak levels of muscle anti-inflammatory macrophages and also consistent with co-culture studies, where increasing numbers of anti-inflammatory macrophages protected myofibers from the pro-atrophy activity of pro-inflammatory macrophages (Figure 6). It is also in line with findings in a hepatocellular carcinoma model of cachexia, where macrophages were found to preserve adipose mass.[41] How anti-inflammatory macrophages protect myofibers in cachexia is not known. These macrophages might secrete factors to protect myofibers by inhibiting the production of E3 ubiquitin ligases or other drivers of catabolism. Alternatively, anti-inflammatory macrophages might act on other cell types within the muscle microenvironment to inhibit their ability to promote cachexia. For example, macrophages are able to signal to FAPs to ensure their depletion during the latter phases of muscle regeneration[42] and FAPs secrete IL-6 to promote muscle atrophy in a denervation model of muscle wasting.[43] Therefore, it is possible that, in cancer cachexia, anti-inflammatory macrophages inhibit procachectic activity of FAPs by limiting IL-6 production. Importantly, while we showed that macrophages exert both pro- and anti-atrophy effects in the cachectic muscle microenvironment, these signals may be independent of other signaling pathways that promote protein catabolism. Consistent with previous findings, Pax7 deletion in MuSCs was sufficient to preserve some muscle mass, but not the loss of mass derived from proteolytic pathways within myofibers.[10] We suspect a similar regulation might be at play with regards to the anti-atrophy effects of macrophages whose activities are overshadowed by pro-atrophy signals emanating from myofibers. This notion is consistent with transplantation experiments performed with *CCR2*$^{-/-}$ bone marrow cells in cachectic mice (Figure 4), where TA muscle mass was unchanged from WT animals with cachexia (data not shown).

Our results also pointed to the accumulation of resident macrophages in cachectic muscle. Little information exists on whether these cells polarize or how they contribute to muscle repair,[44] but future studies will need to address their functional roles in regulating the distinct states of muscle wasting during cachexia.[45] Likewise, our data and others have observed the accumulation of eosinophils and neutrophils in cachectic muscles.[16,17,32,33] Since these cells also express CD11b and were likely eliminated in our DTA experiment (Figure 5), their roles in regulating muscle atrophy and preserving myofibers in cancer will need to be accounted for.

Although this current study reiterates our earlier findings that muscle wasting in cancer associates with skeletal muscle damage,[10,20] admittedly the accumulation of macrophages in cachectic muscle does not compare to that of acute muscle injury.[19] However, co-culture studies revealed that relatively few macrophage are needed to activate NF-κB in myoblasts. This underscores the potency of macrophages and their effectiveness to regulate muscle wasting, suggesting that even a minor pool of infiltrating monocytes or expanding resident cells can have a significant impact on the muscle microenvironment in cancer.

Limitation of the study

Although we determined that accumulating macrophage populations in cachectic muscle consist of both resident and infiltrating cells, we are unable at this point to define how resident macrophages specifically mediate the different states of muscle wasting or how

they contribute to maintaining NF-κB activity in the muscle microenvironment. In addition, although we show considerable similarities between mouse and human single-cell data, we recognize that patients are inherently more heterogeneous, and thus larger cohorts in a separate transcriptomic study will need to be analyzed. Furthermore, while *in vitro* assays were informative, we recognize their shortcoming in not accurately reflecting the heterogeneity of macrophages *in vivo*. Moreover, this study was unable to identify the upstream activators of NF-κB in cachectic muscle. Finally, our study was designed to specially assess males in both animal models and patients but, given the growing acceptance of sexual dimorphism in cancer cachexia,[46] a follow-up study will need to be conducted to determine whether our findings are applicable in females.

STAR★METHODS

RESOURCE AVAILABILITY

Lead contact—Further information and request for resources and reagents should be directed to the lead contact, Dr. Denis Guttridge (guttridg@musc.edu).

Materials availability—Unique reagents generated in this study can be made available upon request to the lead contact after a Materials Transfer Agreement has been completed.

Data and code availability—All raw sequencing data have been deposited on the Gene Expression Omnibus (GEO) database and are publicly available (list in key resources table). Original code has also been described and is available on GitHub. Any additional information required to reanalyze data can be provided by the lead contact on request.

EXPERIMENTAL MODELS AND STUDY PARTICIPANT DETAILS

Mice—All mouse experiments were approved the Medical University of South Carolina Institutional Animal Care and Use Committee under protocol IACUC-2021–01223. Animals were housed with littermates, up to 5 total mice/cage and given *ad libitum* access to a standard show diet and water. Due to sexual dimorphisms in cancer cachexia, only male mice were used in this study.

For the colon-26 (C-26) cancer model, male CD2F1 mice from Charles River (RRID:IMSR_CRL:033) were injected subcutaneously in the right flank with 1×10^6 cells in a volume of 100μL PBS. For the Lewis Lung Carcinoma (LLC) model, male C57BL/6J from Charles River (RRID:IMSR_CRL:027) were injected intramuscularly with 5×10^5 cells in a volume of 100μL PBS in the right gluteus muscle under anesthesia. In both models, control mice were similarly injected with identical volumes of PBS. Mice were euthanized by CO_2 asphyxiation at approximately 21 days post injection when cachexia was evident. For experiments using *Pax7-Cre^{ER}* (RRID:MGI:4436914),[47] *HSA-Cre^{ER}* (RRID:IMSR_JAX:025750)[48] *or PDGFRa-Cre^{ER}* (RRID:IMSR_JAX:032770)[49] animal models crossed with the *IKKβ ^{flf}* (RRID:MGI:2445462)[50] and CCL2 ^{flf} (RRID:IMSR_JAX:016849),[51] LLC tumors were allowed to develop for 10 days, at which time tamoxifen was administered for 5 consecutive days at a concentration of 1mg/10g of body weight to activate Cre recombinase. The KPP model was generated

as previously described.[21] Briefly, male *Kras*$^{LSL\text{-}G12D/+}$ *Pten*$^{f/f}$ mice were bred to female *Ptf1a*$^{ER\text{-}Cre/+}$, *Pten*$^{f/f}$ mice (RRID:IMSR_JAX:008179, RRID:IMSR_JAX:019378 and RRID:IMSR_JAX:006440).[52–54] KPP mice (*Kras*$^{LSL\text{-}G12D/+}$, *Ptf1a*$^{ER\text{-}Cre/+}$, *Pten*$^{f/f}$) were injected with tamoxifen (Sigma) at 24–28 days of age at a dose of 1mg/10g of body weight. Male littermates were utilized as controls and received tamoxifen at the same dosage. Mice were euthanized by CO_2 asphyxiation at endpoints according to IACUC endpoint criteria, including ascites, weight loss, lethargy, or a body score of <1.5, or at specific timepoints.

Cell culture—Cells were cultured at 37°C and 5% CO2 in 10% DMEM (Corning) for C2C12, and RPMI (Corning) for C-26 and LLC cells supplemented with 10% fetal bovine serum (FBS) and 1% of streptomycin/penicillin (Invitrogen). C2C12 myoblasts were differentiated by switching to cell cultures to DMEM supplemented with 2% horse serum for 96h. For the isolation of fibro-adipogenic progenitors, we used protocols described by others.[55,56] Briefly, mononuclear cells were isolated from skeletal muscle using the Miltenyi Skeletal Muscle Dissociation Kit on the gentleMACs Dissociator. Digestion was inactivated with 10% horse serum in DMEM and filtered through 100 μm and 40 μm cell strainers. Cells were then incubated with Dead Cell Removal Beads (Miltenyi) followed by magnetic separation on LS columns (Miltenyi). Cells were incubated with biotin labeled CD45 (Biolegend), Biotin labeled CD31 (Biolegend), biotin labelled α7 integrin (Miltenyi) antibodies, followed by incubation with anti-biotin labelled beads (Miltenyi). Cells were loaded onto LD columns and the effluent fractions were collected and incubated with PE-Ly6A/E antibody, followed by incubated with anti-PE labelled beads. Samples were run through LS Columns and the labelled cells were collected. For culture, FAPs were grown in DMEM containing 20% FBS, 1% pencillin-streptomycin and 2.5 ng/mL bFGF (Invitrogen).

For migration assays, 5×10^4 RAW 264.7 cells were seeded in the top chamber of an 8 μm porous chemotaxis chamber (Corning-Costar, USA), with conditioned media from C2C12s plate in the bottom chamber. Cells were allowed to migrate for 6 h, at which time membranes were fixed in 4% paraformaldehyde and stained with crystal violet. A total of 3 images from each membrane were used to quantitate migration from 3 biological replicates per condition.

Human subjects—Informed consent was obtained from patients with pancreatic cancer undergoing tumor resection surgery or patients that were cancer-free undergoing routine abdominal surgery (ex. Gastric pacemaker, hernia repair). During surgery, muscle tissue was extracted from the abdominal muscle ($1.0cm^3$). Patient samples used for histology were from The Ohio State University (IRB 2010C0051), with patient characteristics summarized in Table S1. Samples for single cell RNA sequencing were collected from Protocol Pro00093400 (MUSC), with patient characteristic summarized in Table S2. Samples for ELISA were collected from both The Ohio State University (IRB 2010C0051) The Ohio State University (IRB 2010C0051), with patient characteristics located in Table S3. Self-reported weight loss as well weight recorded in existing medical records were used to determine cachexia status. Patients with pancreatic cancer with <5% weight loss were

classified as weight stable, whereas a cutoff of >10% weight loss was used to classify patients as cachectic.

METHOD DETAILS

Animal procedures

For muscle specific macrophage ablation, *CD11b-DTR* mice (RRID:IMSR_JAX:006000)[57] were maintained on a C57BL/6 background for LLC cell injection or backcrossed to CD2F1 mice for at least 7 generations for C-26 tumor cell injection. Bromodeoxyuridine/5-bromo-2′-deoxyuridine (BrdU, Sigma) was injected at 8- and 12-day post cell injection to label proliferating cells. Diphtheria toxin (Millipore) was injection intramuscularly in the TA muscle at a dose of 25 ng/g of body weight at 15- and 19-day post tumor cell injection. For systemic macrophage ablation, 100 μL of clodronate or PBS encapsulated liposomes were injected via two intravenous injections on day 15 and 20 post injection tumor cell injection, as well as one intraperitoneal injection on day 18.

Bone marrow transplantation experiments were performed as previously described. Briefly, recipient mice were injected via with busulfan intraperitoneal injection at a concentration of 20 mg/kg for 4 consecutive days. The next day following the last injection, syngeneic donor mice (RRID:IMSR JAX:027619, RRID:IMSR JAX:002014, RRID:IMSR_CRL:027) were euthanized by CO_2 asphyxiation and bone marrow was collected under sterile conditions. Marrow was collected, and cells were filtered through a 40 μm filter and treat with Red Cell Lysis Buffer for 10 min (Sigma). Cells were washed and resuspended concentration of 8×10^6 cells/mL in sterile PBS. Recipient mice then received 300 μL of cellular suspensions via tail vein injections. Mice were allowed to recover for 21 days prior to LLC tumor cell injection.

Real-time RT-PCR and Nanostring nCounter analysis

Hindlimb muscle from cachectic and control mice were snap frozen in liquid nitrogen and homogenized in Trizol reagent (Life Technologies), and mRNA was extracted as per manufacturers protocol. M-MLV Reverse Transcriptase was used for cDNA synthesis (Life Technologies). Real-time PCR was performed on Applied system QuantStudio3 using SYBR Green reagent (Roche). Mouse β-actin was used as a housekeeping gene reference sample. RT-PCR primer sets appear in Table S3. The nCounter Mouse Inflammation V2 Panel Gene List (Nanostring Technologies, XT-CSO-MIN2–12) was used to profile the expression of 254 genes (248 inflammatory genes, 6 housekeeping). A total of 100 ng was used for each sample. Analysis was conducted at the MUSC Hollings Cancer Center Translational Science Lab, and RNA was quantified by nCounter Digital Analyzer.

Immunofluorescence

Muscles were frozen in an isopentane bath cooled in liquid nitrogen and subsequently sectioned on a cryostat at a thickness of 10μm (Leica). Slides were stored at −80°C until use, at which time they were dried at room temperature, fixed in 4% paraformaldehyde, and blocked with 10% donkey serum diluted in PBS. Primary antibody staining was performed overnight at 4°C at antibody specific dilutions, and species-specific Alexa-Fluor secondary

antibodies (Invitrogen) were diluted to 1:500 and incubated for 1 h at room temperature. Images were captured on a Zeiss Axio Imager A2 microscope. For quantification, at least five images from three separate muscle sections, for fifteen images total, were used to assess fiber size, BrdU, and $CD11b^+$ cells. Counts were made in ImageJ.

ELISA

For ELISA on cell culture supernatants, equal number of cells from each C2C12 cell line analyzed were seeded in 3mL of DMEM in biological triplicate. ELISAs for Ccl2, Cxcl1 and Cxcl2 (R&D) was performed on supernatant collected after 24 h as per manufacturers' protocols. For ELISA on tissue, muscles were homogenized in RIPA buffer containing protease and phosphatase inhibitors. Protein concentration was measured by BCA assay and equivalent concentrations (1 mg/mL) of each sample were used for ELISA of TNF, IL-1β and IL-6 as per manufacturer's protocol.

Single cell RNA sequencing

To isolate mononuclear cells for single cell sequencing, we digested 0.5–1 g of hindlimb muscle from 2 cachectic and 2 control mice using the Miltenyi Skeletal Muscle Dissociation Kit on the gentleMACs Dissociator. Digestion was inactivated with 10% horse serum in DMEM and filtered through 100 μm and 40 μm cell strainers. Cachectic and control mice were pooled and cells were incubated with Dead Cell Removal Beads (Miltenyi) followed by magnetic separation on LS columns. The effluent fraction, constituting the live cell fraction, was incubated with CD45 microbeads (Miltenyi). Both the unlabeled (effluent) fraction and the labelled fractions, constituting CD45 negative and positive cell populations respectively, were sent for single cell sequencing. Human muscle biopsies were similarly processed using collagenase/dispase for digestion. For patient samples, 1 control, 2 weight stable PDAC, and 1 cachectic PDAC sample were processed for single cell RNA sequencing (Table S2). For the second weight stable PDAC patient, the number of extracted mononuclear cells was low following isolation, and a considerably low number of cells passed quality control. Thus, this sample was not used for analysis. For the remaining $CD45^-$ samples, cells were used for sequencing in the Control, the first weight stable PDAC patient, and the cachectic PDAC patient. After sequencing, we collapsed the patients with PDAC into one sample due to low reads obtained in the cachectic sample.

Raw sequencing data were processed with CellRanger pipeline (v7.0.0).[58] Cellranger ''mkfastq'' command was used to demultiplex the different samples and Cellranger ''count'' command was used to generate gene – cell expression matrices. Ambient RNA contamination was inferred and removed using CellBender (v0.2.0) with standard parameters. Human Genome hg38 or Mouse Genome mm10 was used for the alignment and gencode.v42 was used for gene annotation and coordinates.[59] Downstream analysis was performed in R with Seurat (v4.3.0)[60] and customized R scripts. CD45 positive and CD45 negative samples from each experiment were merged into separate unique single cell objects. Macrophage and FAPs from positive samples were subset and re-clustered using SCTransform workflow using 30 principal components and resolution of 0.4 for Louvain clustering and UMAP. For C-26 analysis, the single cell RNA sequencing experiment was performed in duplicate, samples were concatenated and results were combined, with the

exception of the control CD45^{-} samples, which did not pass quality control. Cell annotation was performed using gene markers by manually curation.

Flow cytometry

Mononuclear cells were isolated from hindlimb muscles as described for single cell RNA sequencing. Following Dead Cell Removal, isolated cells were washed in FACs buffer and fixed in FACS buffer containing 3.7% formaldehyde for 30 min on ice. Mouse spleens were crushed with an end of 3mL syringe in 5mL PBS and then passed through 40 μM cell strainer. Cells were centrifuged to remove supernatant and resuspended in 10 mL ice-cold RBC lysis buffer (Sigma) for 10 min at room temperature. After RBC lysis, 30 mL of PBS was added into the RBC lysis buffer and cells were centrifuged to remove supernatant (RBC lysis buffer). After PBS wash for another time, isolated spleen cells were fixed in FACS buffer contain 3.7% formaldehyde for 30 min on ice. Fixed muscle mononuclear cells and spleen cells were centrifuged to remove formaldehyde and subsequently washed with PBS for once and stored in PBS at 4°C before use. Before staining for flow cytometer analysis, mononuclear cells and 1 million cells per tube of spleen cells were centrifuged in a microcentrifuge tube and resuspended in 100 μL blocking solution (10% Rat serum (Millipore)/FACS buffer containing 0.5 μg anti-mouse CD16/CD32 (biolegend) and incubated for 30 min on ice. After blocking, an antibody cocktails (Figures S1B, S4C, and S5L) were added into muscle mononuclear cells and single antibodies were added into each tube of spleen cells according to the manufacturer, or in the case of skeletal muscle resident macrophages, from cited reports.[25,44,61] After overnight incubations on ice, stained cells were washed in PBS twice and resuspended in 0.8–1.0 mL FACS buffer and analyzed by Fortessa X-20 flow cytometry with single antibody-stained spleen cells as color compensation control. All muscle nuclear samples were run through flow cytometer analysis. If a sample reach stopping threshold too early without using up all sample solutions, total cell number will be adjusted as total cell # = (acquired cell #/volume analyzed).

Crispr/Cas9 gene editing

For knockout of specific chemokines, we used CHOPCHOP to design guide RNAs for *Ccl2*, *Cxcl1* and *Cxcl2* (Table S4), which were then cloned into the lentiCRISPRv2 vector (Addgene #104990). Lentivirus was produced in 293Ts by co-transfecting Lenticas9 (Addgene, #52962) with either sgRNAs or scramble lentiCRISPRv2. C2C12s were infected with lentivirus and maintained under selection until experiments were performed.

Bone marrow derived macrophage isolation

For bone marrow derived macrophages, 4–8-week-old mice from B6, *TNF*$^{-/-}$ and *IL-1β*$^{-/-}$ mice (RRID:IMSR_CRL:027, RRID:IMSR_JAX:034447, RRID:IMSR_JAX:003008)[62,63] were euthanized and hindlimb bones were extracted under sterile conditions and placed in 10% FBS media. In the tissue culture hood, marrow was extracted by flushing the bone with 10 mL of media through and 27-gauge needle. Cells were collected and run through and 18-gauge needle to break apart aggregates, incubated with RBC lysis buffer, and cultured in 10% HyClone FBS supplemented with M-CSF-1 (25 ng/mL). After five days, LPS and

IFNγ were added to induce M1 polarization. The following day, IL-4 and IL-13 were added for an additional 24 h to induce M2-like polarization.

QUANTIFICATION AND STATISTICAL ANALYSIS

Data are presented as mean with all individual datapoints shown, with standard error of the mean represented. Statistical analyses were initially analyzed with GraphPad Prism. Comparisons between two groups were carried out using Student's t-test or Welch's t test. Multiple group comparisons were carried out using one-way ANOVA with Dunnett's test or Welch's ANOVA and has been indicated in figure legends. Number of samples used, and significance is recorded in figure legends.

Supplementary Material

Refer to Web version on PubMed Central for supplementary material.

ACKNOWLEDGMENTS

We thank members of the Guttridge laboratory for their helpful discussions throughout this study. We are also grateful to members of our PDAC cachexia P01 team for their continuing support and feedback given to this project, as well as The Ohio State University Comprehensive Cancer Center Cancer Cachexia Program, who provided patient samples. We thank Dr. Michael Karin for sharing *IKKβ* conditional mice, as well as other colleagues who generated the mutant mice used in our study. Funding support was provided by an NIH/NIAMS R01 grant AR072714 to D.C.G., J.G.T., and D.J.W.; a Hollings Cancer Center Postdoctoral Fellowship Award to B.R.P.; an NIH/NCI F30 grant CA265071 to A.O.; an NIH/NIAMS R00 grant AR071508 to E.E.T.; NIH/NCI R01 grants CA122596 and CA194593, VA awards I01BX004177 and I01CX002046, an NIH/NCI P30 Cancer Center Support Grant P30 CA082709 to T.A.Z; an NIH/NCI P30 Cancer Center Support Grant CA138313 to M.C.O. and D.C.G.; and an NIH/NCI P01 grant CA236778 to T.A.Z., M.C.O., and D.C.G.

REFERENCES

1. Fearon K, Strasser F, Anker SD, Bosaeus I, Bruera E, Fainsinger RL, Jatoi A, Loprinzi C, MacDonald N, Mantovani G, et al. (2011). Definition and classification of cancer cachexia: an international consensus. Lancet Oncol. 12, 489–495. 10.1016/S1470-2045(10)70218-7. [PubMed: 21296615]
2. Argiles JM, Busquets S, Stemmler B, and Lopez-Soriano FJ (2014). Cancer cachexia: understanding the molecular basis. Nat. Rev. Cancer 14, 754–762. 10.1038/nrc3829. [PubMed: 25291291]
3. Siegel RL, Giaquinto AN, and Jemal A (2024). Cancer statistics, 2024. CA. Cancer J. Clin. 74, 12–49. 10.3322/caac.21820.
4. Bachmann J, Heiligensetzer M, Krakowski-Roosen H, Büchler MW, Friess H, and Martignoni ME (2008). Cachexia worsens prognosis in patients with resectable pancreatic cancer. J. Gastrointest. Surg. 12, 1193–1201. 10.1007/s11605-008-0505-z. [PubMed: 18347879]
5. Nemer L, Krishna SG, Shah ZK, Conwell DL, Cruz-Monserrate Z, Dillhoff M, Guttridge DC, Hinton A, Manilchuk A, Pawlik TM, et al. (2017). Predictors of Pancreatic Cancer-Associated Weight Loss and Nutritional Interventions. Pancreas 46, 1152–1157. 10.1097/MPA.0000000000000898. [PubMed: 28902785]
6. Wakabayashi H, Arai H, and Inui A (2023). Anamorelin in Japanese patients with cancer cachexia: an update. Curr. Opin. Support. Palliat. Care 17, 162–167. 10.1097/SPC.0000000000000658. [PubMed: 37389636]
7. Acharyya S, Ladner KJ, Nelsen LL, Damrauer J, Reiser PJ, Swoap S, and Guttridge DC (2004). Cancer cachexia is regulated by selective targeting of skeletal muscle gene products. J. Clin. Invest. 114, 370–378. 10.1172/jci20174. [PubMed: 15286803]
8. Sandri M (2016). Protein breakdown in cancer cachexia. Semin. Cell Dev. Biol. 54, 11–19. 10.1016/j.semcdb.2015.11.002. [PubMed: 26564688]

9. de Fatima Silva F, de Morais H, Ortiz Silva M, da Silva FG, Vianna Croffi R, Serrano-Nascimento C, Rodrigues Graciano MF, Rafael Carpinelli A, Barbosa Bazotte R, and de Souza HM (2020). Akt activation by insulin treatment attenuates cachexia in Walker-256 tumor-bearing rats. J. Cell. Biochem. 121, 4558–4568. 10.1002/jcb.29682. [PubMed: 32056265]
10. He WA, Berardi E, Cardillo VM, Acharyya S, Aulino P, Thomas-Ahner J, Wang J, Bloomston M, Muscarella P, Nau P, et al. (2013). NF-kappaB-mediated Pax7 dysregulation in the muscle microenvironment promotes cancer cachexia. J. Clin. Invest. 123, 4821–4835. 10.1172/JCI68523. [PubMed: 24084740]
11. Cahlin C, Körner A, Axelsson H, Wang W, Lundholm K, and Svanberg E (2000). Experimental cancer cachexia: the role of host-derived cytokines interleukin (IL)-6, IL-12, interferon-gamma, and tumor necrosis factor alpha evaluated in gene knockout, tumor-bearing mice on C57 Bl background and eicosanoid-dependent cachexia. Cancer Res. 60, 5488–5493. [PubMed: 11034092]
12. Ramsey ML, Talbert E, Ahn D, Bekaii-Saab T, Badi N, Bloomston PM, Conwell DL, Cruz-Monserrate Z, Dillhoff M, Farren MR, et al. (2019). Circulating interleukin-6 is associated with disease progression, but not cachexia in pancreatic cancer. Pancreatology 19, 80–87. 10.1016/j.pan.2018.11.002. [PubMed: 30497874]
13. Talbert EE, Lewis HL, Farren MR, Ramsey ML, Chakedis JM, Rajasekera P, Haverick E, Sarna A, Bloomston M, Pawlik TM, et al. (2018). Circulating monocyte chemoattractant protein-1 (MCP-1) is associated with cachexia in treatment-naive pancreatic cancer patients. J. Cachexia Sarcopenia Muscle 9, 358–368. 10.1002/jcsm.12251. [PubMed: 29316343]
14. Hou YC, Wang CJ, Chao YJ, Chen HY, Wang HC, Tung HL, Lin JT, and Shan YS (2018). Elevated Serum Interleukin-8 Level Correlates with Cancer-Related Cachexia and Sarcopenia: An Indicator for Pancreatic Cancer Outcomes. J. Clin. Med. 7, 502. 10.3390/jcm7120502. [PubMed: 30513776]
15. Rupert JE, Narasimhan A, Jengelley DH, Jiang Y, Liu J, Au E, Silverman LM, Sandusky G, Bonetto A, Cao S, et al. (2021). Tumor-derived IL-6 and trans-signaling among tumor, fat, and muscle mediate pancreatic cancer cachexia. J. Exp. Med. 218, e20190450. 10.1084/jem.20190450.
16. Machado AP, Costa Rosa LFPB, and Seelaender MCL (2004). Adipose tissue in Walker 256 tumour-induced cachexia: possible association between decreased leptin concentration and mononuclear cell infiltration. Cell Tissue Res. 318, 503–514. 10.1007/s00441-004-0987-2. [PubMed: 15490241]
17. Burfeind KG, Zhu X, Norgard MA, Levasseur PR, Huisman C, Buenafe AC, Olson B, Michaelis KA, Torres ER, Jeng S, et al. (2020). Circulating myeloid cells invade the central nervous system to mediate cachexia during pancreatic cancer. Elife 9, e54095. 10.7554/eLife.54095.
18. Shukla SK, Markov SD, Attri KS, Vernucci E, King RJ, Dasgupta A, Grandgenett PM, Hollingsworth MA, Singh PK, Yu F, and Mehla K (2020). Macrophages potentiate STAT3 signaling in skeletal muscles and regulate pancreatic cancer cachexia. Cancer Lett. 484, 29–39. 10.1016/j.canlet.2020.04.017. [PubMed: 32344015]
19. Tidball JG (2017). Regulation of muscle growth and regeneration by the immune system. Nat. Rev. Immunol. 17, 165–178. 10.1038/nri.2016.150. [PubMed: 28163303]
20. Acharyya S, Butchbach MER, Sahenk Z, Wang H, Saji M, Carathers M, Ringel MD, Skipworth RJE, Fearon KCH, Hollingsworth MA, et al. (2005). Dystrophin glycoprotein complex dysfunction: a regulatory link between muscular dystrophy and cancer cachexia. Cancer Cell 8, 421–432. 10.1016/j.ccr.2005.10.004. [PubMed: 16286249]
21. Talbert EE, Cuitino MC, Ladner KJ, Rajasekerea PV, Siebert M, Shakya R, Leone GW, Ostrowski MC, Paleo B, Weisleder N, et al. (2019). Modeling Human Cancer-induced Cachexia. Cell Rep. 28, 1612–1622.e1614. 10.1016/j.celrep.2019.07.016. [PubMed: 31390573]
22. Kim S, Iizuka K, Kang HSP, Dokun A, French AR, Greco S, and Yokoyama WM (2002). In vivo developmental stages in murine natural killer cell maturation. Nat. Immunol. 3, 523–528. 10.1038/ni796. [PubMed: 12006976]
23. Chazaud B, Sonnet C, Lafuste P, Bassez G, Rimaniol AC, Poron F, Authier FJ, Dreyfus PA, and Gherardi RK (2003). Satellite cells attract monocytes and use macrophages as a support to escape apoptosis and enhance muscle growth. J. Cell Biol. 163, 1133–1143. 10.1083/jcb.200212046. [PubMed: 14662751]

24. Acharyya S, Villalta SA, Bakkar N, Bupha-Intr T, Janssen PML, Carathers M, Li ZW, Beg AA, Ghosh S, Sahenk Z, et al. (2007). Interplay of IKK/NF-kappaB signaling in macrophages and myofibers promotes muscle degeneration in Duchenne muscular dystrophy. J. Clin. Invest. 117, 889–901. 10.1172/JCI30556. [PubMed: 17380205]
25. De Micheli AJ, Laurilliard EJ, Heinke CL, Ravichandran H, Fraczek P, Soueid-Baumgarten S, De Vlaminck I, Elemento O, and Cosgrove BD (2020). Single-Cell Analysis of the Muscle Stem Cell Hierarchy Identifies Heterotypic Communication Signals Involved in Skeletal Muscle Regeneration. Cell Rep. 30, 3583–3595.e5. 10.1016/j.celrep.2020.02.067. [PubMed: 32160558]
26. Mantovani A, and Sica A (2010). Macrophages, innate immunity and cancer: balance, tolerance, and diversity. Curr. Opin. Immunol. 22, 231–237. 10.1016/j.coi.2010.01.009. [PubMed: 20144856]
27. Wang CH, Shen YC, Hsieh JJ, Yeh KY, and Chang JWC (2006). Clodronate alleviates cachexia and prolongs survival in nude mice xenografted with an anaplastic thyroid carcinoma cell line. J. Endocrinol. 190, 415–423. 10.1677/joe.1.06490. [PubMed: 16899574]
28. Arnold L, Henry A, Poron F, Baba-Amer Y, van Rooijen N, Plonquet A, Gherardi RK, and Chazaud B (2007). Inflammatory monocytes recruited after skeletal muscle injury switch into antiinflammatory macrophages to support myogenesis. J. Exp. Med. 204, 1057–1069. 10.1084/jem.20070075. [PubMed: 17485518]
29. Vogl T, Tenbrock K, Ludwig S, Leukert N, Ehrhardt C, van Zoelen MAD, Nacken W, Foell D, van der Poll T, Sorg C, and Roth J (2007). Mrp8 and Mrp14 are endogenous activators of Toll-like receptor 4, promoting lethal, endotoxin-induced shock. Nat. Med. 13, 1042–1049. 10.1038/nm1638. [PubMed: 17767165]
30. Foell D, and Roth J (2004). Proinflammatory S100 proteins in arthritis and autoimmune disease. Arthritis Rheum. 50, 3762–3771. 10.1002/art.20631. [PubMed: 15593206]
31. Wang X, Sathe AA, Smith GR, Ruf-Zamojski F, Nair V, Lavine KJ, Xing C, Sealfon SC, and Zhou L (2020). Heterogeneous origins and functions of mouse skeletal muscle-resident macrophages. Proc. Natl. Acad. Sci. USA 117, 20729–20740. 10.1073/pnas.1915950117. [PubMed: 32796104]
32. Deyhle MR, Callaway CS, Neyroud D, D'Lugos AC, Judge SM, and Judge AR (2022). Depleting Ly6G Positive Myeloid Cells Reduces Pancreatic Cancer-Induced Skeletal Muscle Atrophy. Cells 11, 1893. 10.3390/cells11121893. [PubMed: 35741022]
33. Petruzzelli M, Ferrer M, Schuijs MJ, Kleeman SO, Mourikis N, Hall Z, Perera D, Raghunathan S, Vacca M, Gaude E, et al. (2022). Early Neutrophilia Marked by Aerobic Glycolysis Sustains Host Metabolism and Delays Cancer Cachexia. Cancers 14, 963. 10.3390/cancers14040963. [PubMed: 35205709]
34. das Neves RX, Yamashita AS, Riccardi DMR, Köhn-Gaone J, Camargo RG, Neto NI, Caetano D, Gomes SP, Santos FH, Lima JDCC, et al. (2023). Cachexia causes time-dependent activation of the inflammasome in the liver. J. Cachexia Sarcopenia Muscle 14, 1621–1630. 10.1002/jcsm.13236. [PubMed: 37177862]
35. Mourkioti F, Kratsios P, Luedde T, Song YH, Delafontaine P, Adami R, Parente V, Bottinelli R, Pasparakis M, and Rosenthal N (2006). Targeted ablation of IKK2 improves skeletal muscle strength, maintains mass, and promotes regeneration. J. Clin. Invest. 116, 2945–2954. 10.1172/JCI28721. [PubMed: 17080195]
36. Cai D, Frantz J, Tawa NE Jr., Melendez PA, Oh BC, Lidov HG, Hasselgren PO, Frontera WR, Lee J, Glass DJ, and Shoelson SE (2004). IKKbeta/NF-kappaB activation causes severe muscle wasting in mice. Cell 119, 285–298. 10.1016/j.cell.2004.09.027. [PubMed: 15479644]
37. Zhang Y, Yang P, Cui R, Zhang M, Li H, Qian C, Sheng C, Qu S, and Bu L (2015). Eosinophils Reduce Chronic Inflammation in Adipose Tissue by Secreting Th2 Cytokines and Promoting M2 Macrophages Polarization. Int. J. Endocrinol. 2015, 565760. 10.1155/2015/565760.
38. Ratnayake D, Nguyen PD, Rossello FJ, Wimmer VC, Tan JL, Galvis LA, Julier Z, Wood AJ, Boudier T, Isiaku AI, et al. (2021). Macrophages provide a transient muscle stem cell niche via NAMPT secretion. Nature 591, 281–287. 10.1038/s41586-021-03199-7. [PubMed: 33568815]
39. Coulis G, Jaime D, Guerrero-Juarez C, Kastenschmidt JM, Farahat PK, Nguyen Q, Pervolarakis N, McLinden K, Thurlow L, Movahedi S, et al. (2023). Single-cell and spatial transcriptomics identify a macrophage population associated with skeletal muscle fibrosis. Sci. Adv. 9, eadd9984. 10.1126/sciadv.add9984.

40. Guttridge DC, Mayo MW, Madrid LV, Wang CY, and Baldwin AS Jr. (2000). NF-kappaB-induced loss of MyoD messenger RNA: possible role in muscle decay and cachexia. Science 289, 2363–2366. 10.1126/science.289.5488.2363. [PubMed: 11009425]
41. Erdem M, Möckel D, Jumpertz S, John C, Fragoulis A, Rudolph I, Wulfmeier J, Springer J, Horn H, Koch M, et al. (2019). Macrophages protect against loss of adipose tissue during cancer cachexia. J. Cachexia Sarcopenia Muscle 10, 1128–1142. 10.1002/jcsm.12450. [PubMed: 31318182]
42. Lemos DR, Babaeijandaghi F, Low M, Chang CK, Lee ST, Fiore D, Zhang RH, Natarajan A, Nedospasov SA, and Rossi FMV (2015). Nilotinib reduces muscle fibrosis in chronic muscle injury by promoting TNF-mediated apoptosis of fibro/adipogenic progenitors. Nat. Med. 21, 786–794. 10.1038/nm.3869. [PubMed: 26053624]
43. Madaro L, Passafaro M, Sala D, Etxaniz U, Lugarini F, Proietti D, Alfonsi MV, Nicoletti C, Gatto S, De Bardi M, et al. (2018). Denervation-activated STAT3-IL-6 signalling in fibro-adipogenic progenitors promotes myofibres atrophy and fibrosis. Nat. Cell Biol. 20, 917–927. 10.1038/s41556-018-0151-y. [PubMed: 30050118]
44. Brigitte M, Schilte C, Plonquet A, Baba-Amer Y, Henri A, Charlier C, Tajbakhsh S, Albert M, Gherardi RK, and Chrétien F (2010). Muscle resident macrophages control the immune cell reaction in a mouse model of notexin-induced myoinjury. Arthritis Rheum. 62, 268–279. 10.1002/art.27183. [PubMed: 20039420]
45. Wang X, and Zhou L (2022). The Many Roles of Macrophages in Skeletal Muscle Injury and Repair. Front. Cell Dev. Biol. 10, 952249. 10.3389/fcell.2022.952249.
46. Zhong X, and Zimmers TA (2020). Sex Differences in Cancer Cachexia. Curr. Osteoporos. Rep. 18, 646–654. 10.1007/s11914-020-00628-w. [PubMed: 33044689]
47. Nishijo K, Hosoyama T, Bjornson CRR, Schaffer BS, Prajapati SI, Bahadur AN, Hansen MS, Blandford MC, McCleish AT, Rubin BP, et al. (2009). Biomarker system for studying muscle, stem cells, and cancer in vivo. FASEB J 23, 2681–2690. 10.1096/fj.08-128116. [PubMed: 19332644]
48. McCarthy JJ, Srikuea R, Kirby TJ, Peterson CA, and Esser KA (2012). Inducible Cre transgenic mouse strain for skeletal muscle-specific gene targeting. Skelet. Muscle 2, 8. 10.1186/2044-5040-2-8. [PubMed: 22564549]
49. Chung MI, Bujnis M, Barkauskas CE, Kobayashi Y, and Hogan BLM (2018). Niche-mediated BMP/SMAD signaling regulates lung alveolar stem cell proliferation and differentiation. Development 145, dev163014. 10.1242/dev.163014.
50. Park JM, Greten FR, Li ZW, and Karin M (2002). Macrophage apoptosis by anthrax lethal factor through p38 MAP kinase inhibition. Science 297, 2048–2051. 10.1126/science.1073163. [PubMed: 12202685]
51. Shi C, Jia T, Mendez-Ferrer S, Hohl TM, Serbina NV, Lipuma L, Leiner I, Li MO, Frenette PS, and Pamer EG (2011). Bone marrow mesenchymal stem and progenitor cells induce monocyte emigration in response to circulating toll-like receptor ligands. Immunity 34, 590–601. 10.1016/j.immuni.2011.02.016. [PubMed: 21458307]
52. Jackson EL, Willis N, Mercer K, Bronson RT, Crowley D, Montoya R, Jacks T, and Tuveson DA (2001). Analysis of lung tumor initiation and progression using conditional expression of oncogenic K-ras. Genes Dev. 15, 3243–3248. 10.1101/gad.943001. [PubMed: 11751630]
53. Kopinke D, Brailsford M, Pan FC, Magnuson MA, Wright CVE, and Murtaugh LC (2012). Ongoing Notch signaling maintains phenotypic fidelity in the adult exocrine pancreas. Dev. Biol. 362, 57–64. 10.1016/j.ydbio.2011.11.010. [PubMed: 22146645]
54. Lesche R, Groszer M, Gao J, Wang Y, Messing A, Sun H, Liu X, and Wu H (2002). Cre/loxP-mediated inactivation of the murine Pten tumor suppressor gene. Genesis 32, 148–149. 10.1002/gene.10036. [PubMed: 11857804]
55. Judson RN, Low M, Eisner C, and Rossi FM (2017). Isolation, Culture, and Differentiation of Fibro/Adipogenic Progenitors (FAPs) from Skeletal Muscle. Methods Mol. Biol. 1668, 93–103. 10.1007/978-1-4939-7283-8_7. [PubMed: 28842904]

56. Zhao L, Son JS, Wang B, Tian Q, Chen Y, Liu X, de Avila JM, Zhu MJ, and Du M (2020). Retinoic acid signalling in fibro/adipogenic progenitors robustly enhances muscle regeneration. EBioMedicine 60, 103020. 10.1016/j.ebiom.2020.103020.
57. Duffield JS, Forbes SJ, Constandinou CM, Clay S, Partolina M, Vuthoori S, Wu S, Lang R, and Iredale JP (2005). Selective depletion of macrophages reveals distinct, opposing roles during liver injury and repair. J. Clin. Invest. 115, 56–65. 10.1172/JCI22675. [PubMed: 15630444]
58. Zheng GXY, Terry JM, Belgrader P, Ryvkin P, Bent ZW, Wilson R, Ziraldo SB, Wheeler TD, McDermott GP, Zhu J, et al. (2017). Massively parallel digital transcriptional profiling of single cells. Nat. Commun. 8, 14049. 10.1038/ncomms14049. [PubMed: 28091601]
59. Frankish A, Diekhans M, Jungreis I, Lagarde J, Loveland JE, Mudge JM, Sisu C, Wright JC, Armstrong J, Barnes I, et al. (2021). Gencode 2021. Nucleic Acids Res. 49, D916–D923. 10.1093/nar/gkaa1087. [PubMed: 33270111]
60. Hao Y, Hao S, Andersen-Nissen E, Mauck WM 3rd, Zheng S, Butler A, Lee MJ, Wilk AJ, Darby C, Zager M, et al. (2021). Integrated analysis of multimodal single-cell data. Cell 184, 3573–3587.e29. 10.1016/j.cell.2021.04.048. [PubMed: 34062119]
61. Li YH, Zhang Y, Pan G, Xiang LX, Luo DC, and Shao JZ (2022). Occurrences and Functions of Ly6C(hi) and Ly6C(lo) Macrophages in Health and Disease. Front. Immunol. 13, 901672. 10.3389/fimmu.2022.901672.
62. Shornick LP, De Togni P, Mariathasan S, Goellner J, Strauss-Schoenberger J, Karr RW, Ferguson TA, and Chaplin DD (1996). Mice deficient in IL-1beta manifest impaired contact hypersensitivity to trinitrochlorobenzone. J. Exp. Med. 183, 1427–1436. 10.1084/jem.183.4.1427. [PubMed: 8666901]
63. Pasparakis M, Alexopoulou L, Episkopou V, and Kollias G (1996). Immune and inflammatory responses in TNF alpha-deficient mice: a critical requirement for TNF alpha in the formation of primary B cell follicles, follicular dendritic cell networks and germinal centers, and in the maturation of the humoral immune response. J. Exp. Med. 184, 1397–1411. 10.1084/jem.184.4.1397. [PubMed: 8879212]

Highlights

- Cancer cachexia exhibits muscle inflammation, regulated by NF-κB from multiple cell types
- Muscle inflammation in cancer cachexia is mediated by myeloid cells, mostly macrophages
- Macrophages in cachectic muscle derive from infiltrating monocytes and resident cells
- Heterogeneous populations of macrophages exhibit both pro- and anti-atrophy activities

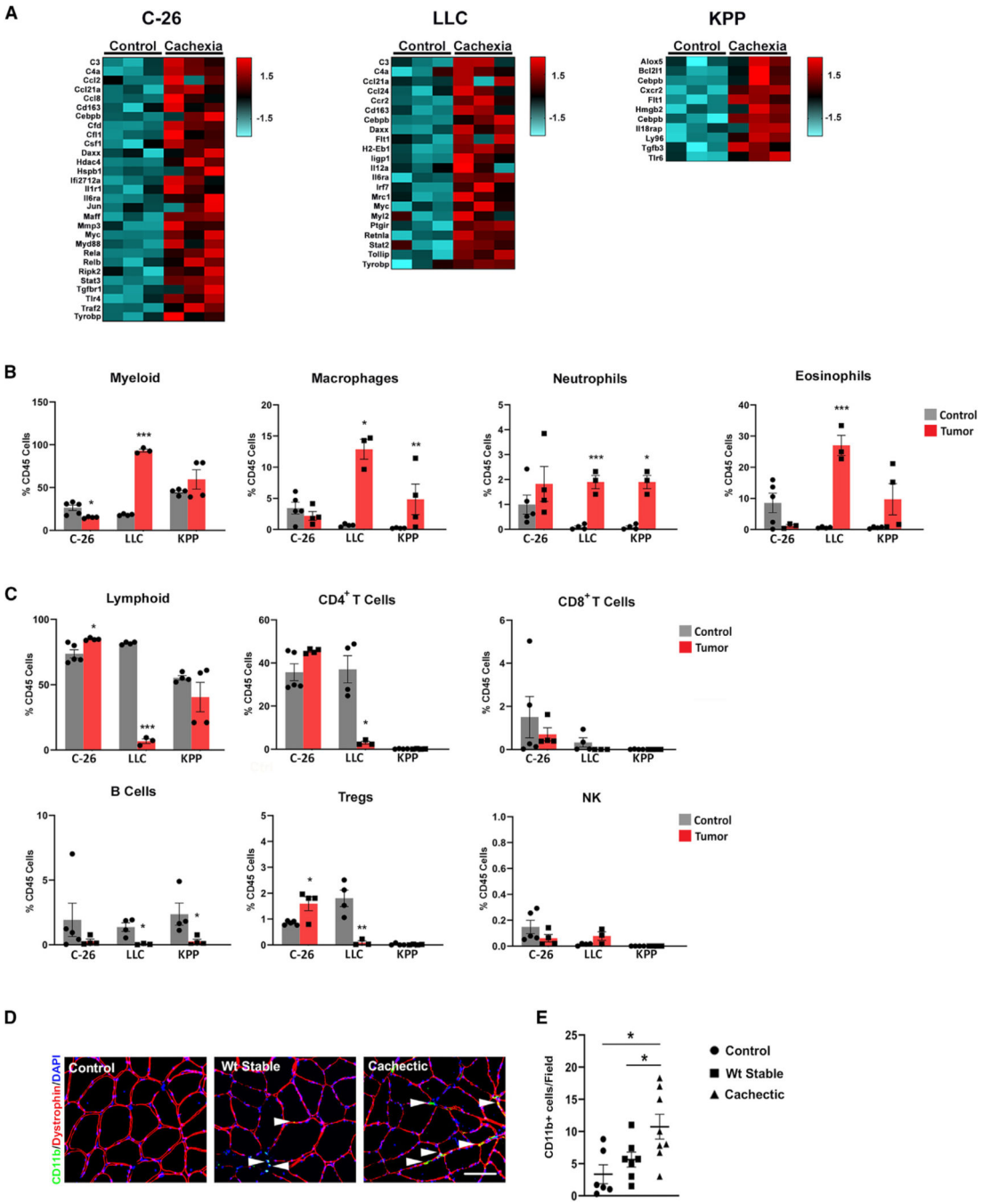

Figure 1. Muscle inflammation in cancer cachexia associates with macrophage accumulation

(A) Heatmaps of significant altered inflammatory genes ($p < 0.05$) probed from TA from cachexia mouse models ($n = 3$).

(B) Flow cytometry analysis of the percentage of myeloid cells as a proportion of $CD45^+$ cells in cachexia models ($n = 3–5$).

(C) Flow cytometry analysis on lymphoid cells in cachexia models ($n = 3–5$).

(D) CD11b (arrowheads) and dystrophin staining from non-cancer control patients, patients with PDAC that were weight stable, and patients with PDAC that were cachectic. Scale bars, 50 μm.

(E) Total number of $CD11b^+$ cells/field for control patients ($n = 6$), WT ($n = 7$), and cachectic ($n = 8$) patients; $*p < 0.05$, $**p < 0.01$. Comparisons to control groups were carried out using Student's t test or Welch's t test. Multiple group comparisons were carried out using one-way ANOVA with Dunnett's test. Bars are ± SEM.

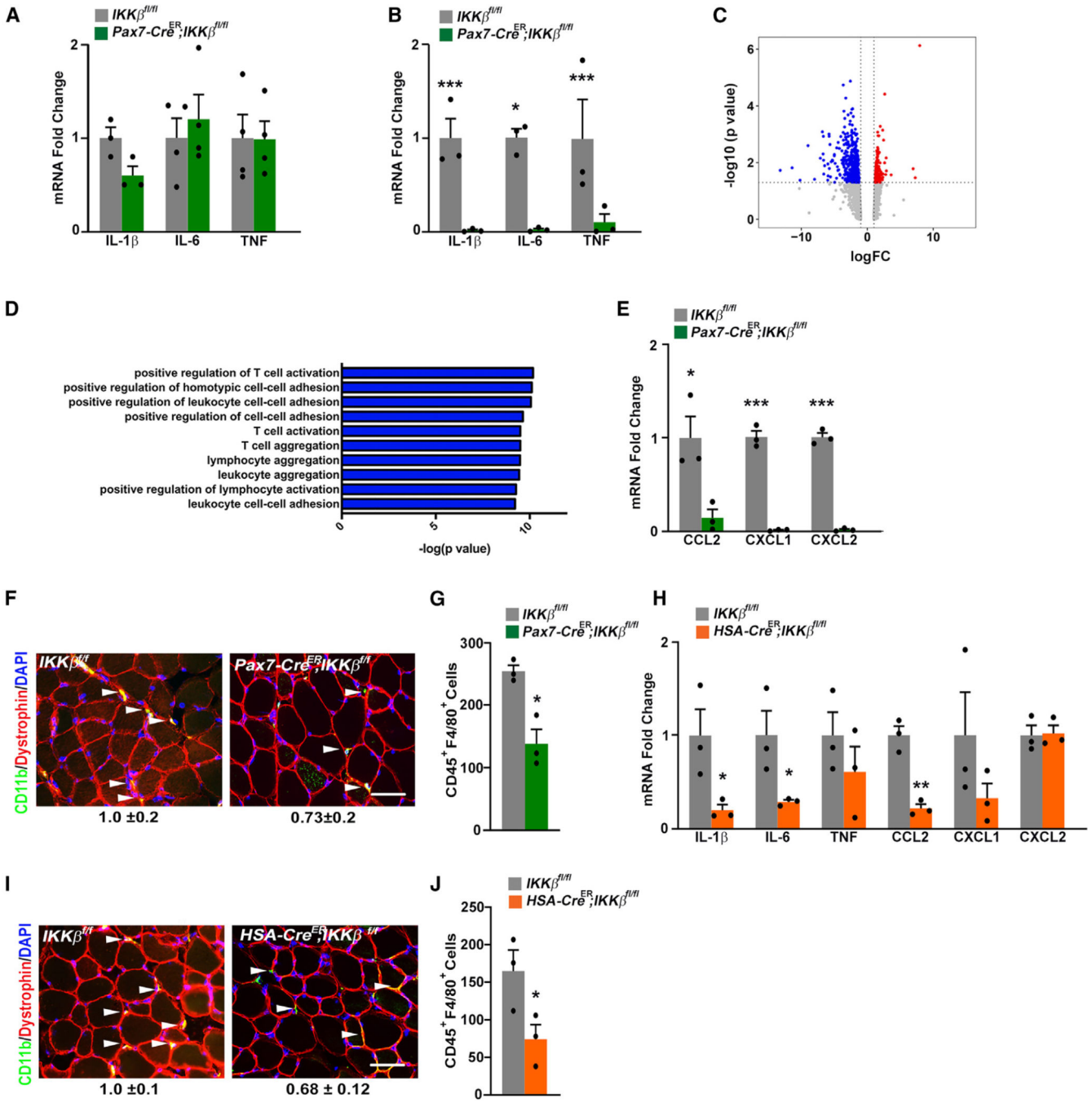

Figure 2. NF-κB functions in MuSCs and myofibers to regulate macrophage accumulation in cancer cachexia

(A) Expression of cytokines from LLC *IKKβ* $^{fl/fl}$ or *Pax7-Cre*^{ER}*; IKKβ* $^{fl/fl}$ mice in TA muscle (n = 4/genotype).

(B) Similar to (A) with the exception that gene expression was performed from mononuclear cells from hindlimb muscles (n = 3/genotype).

(C) Volcano plot from RNA-seq analysis on mononuclear cells from LLC *IKKβ* $^{fl/fl}$ or *Pax7-Cre*^{ER}*; IKKβ* $^{fl/fl}$ (n = 3/genotype) mice.

(D) Gene Ontology analysis from RNA-seq analysis of similar samples to (B) (n = 3/genotype).
(E) Chemokine expression in mononuclear cells from hindlimb muscles of LLC tumor-bearing *IKKβ* $^{fl/fl}$ or *Pax7-Cre*^{ER}*; IKKβ* $^{fl/fl}$ mice (n = 3/genotype).
(F) Immunofluorescence for CD11b and dystrophin on GAST from LLC *IKKβ* $^{fl/fl}$ or *Pax7-Cre*^{ER}*; IKKβ* $^{fl/fl}$ mice, with respective fold changes shown for CD11b^{+} cells/field (n = 3/genotype). Scale bar, 50 μm.
(G) Flow cytometry analysis of CD45^{+} and F4/80^{+} mononuclear cells from hindlimb muscles of LLC *Pax7-Cre*^{ER}; *IKKβ* $^{fl/fl}$ mice (n = 3/genotype).
(H) Cytokines and chemokine expression from TA of LLC *IKKβ* $^{fl/fl}$ or *HSA-Cre*^{ER}*; IKKβ* $^{fl/fl}$ mice (n = 3/genotype).
(I) Immunofluorescence for CD11b and dystrophin on GAST from LLC *IKKβ* $^{fl/fl}$ or *HSA-Cre*^{ER}*; IKKβ* $^{fl/fl}$ mice, with respective fold changes shown in CD11b^{+} cells/field (n = 3/genotype).
(J) Flow cytometry analysis of CD45^{+} and F4/80^{+} mononuclear cells, from hindlimb muscles of LLC *HSA-Cre*^{ER}; *IKKβ* $^{fl/fl}$ mice (n = 3/genotype). Scale bar, 50 μm;*p < 0.05, **p < 0.01, and ***p < 0.001. Comparisons to *IKKβ*$^{fl/fl}$ groups were carried out using Student's t test. Bars are ± SEM.

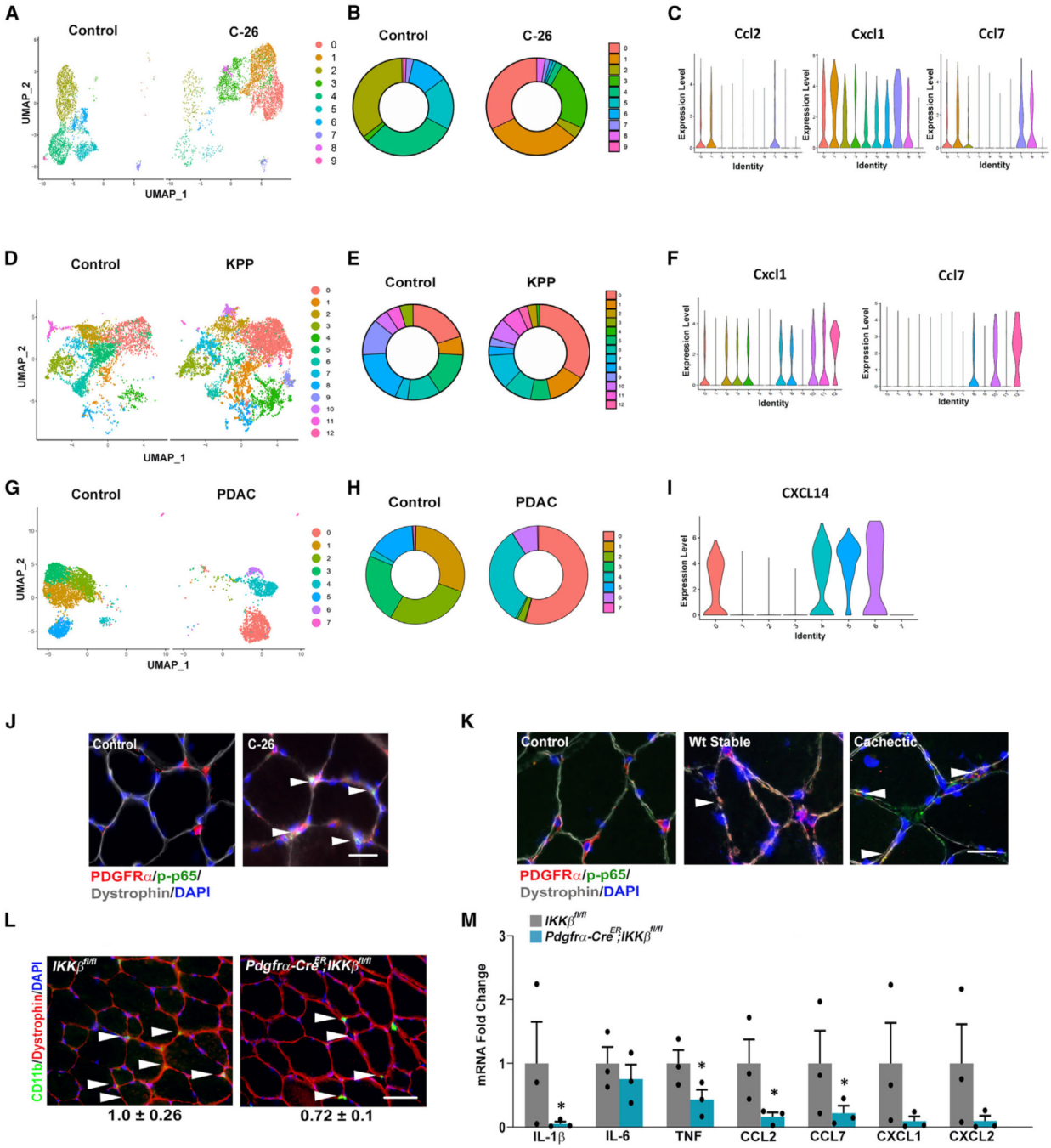

Figure 3. Activated FAPs in cachectic muscle contain NF-κB that regulates macrophage accumulation

(A) UMAP of re-clustered FAPs generated from CD45⁻ cell populations from control and C-26 muscles.

(B) Proportion of FAP populations in (A) from control and C-26 muscles.

(C) Violin plots of inflammatory genes in FAP populations.

(D) UMAP of re-clustered FAPs generated from control and KPP muscles.

(E) Proportion of FAP populations in (D) from control and KPP muscles.

(F) Violin plots of inflammatory genes in FAP populations.

(G) UMAP of re-clustered FAPs generated from $CD45^-$ cells in muscle from control and PDAC patient muscle.
(H) Proportion of FAP populations in (G) from control and patients with PDAC.
(I) Violin plots of inflammatory genes in FAP populations from patient samples.
(J) Immunofluorescence staining of phosphorylated-(p) p65, PDGFRα, and dystrophin on TA from control and C-26 muscles. Scale bar, 10 μm.
(K) Representative immunofluorescence staining of pp65, PDGFRα, and dystrophin on biopsy muscle samples from control, patients that were WT stable, and patients that were cachectic. Scale bar, 10 μm.
(L) Immunostaining for CD11b (arrowheads) and dystrophin on TA samples from LLC *IKKβ* $^{fl/fl}$ or *PDGFRα-Cre*^{ER}*; IKKβ* $^{fl/fl}$ mice, with respective fold changes shown for $CD11b^+$ cells/field (n = 3/genotype). Scale bar, 50 μm.
(M) TNF, IL-1β, IL-6, CCL2, CCL7, CXCL1, and CXCL2 expression was determined from TA in LLC *IKKβ* $^{fl/fl}$ or *PDGFRα-Cre*^{ER}*; IKKβ* $^{fl/fl}$ mice (n = 3/genotype); $*p < 0.05$. Comparisons between two groups were carried out using Student's t test or Welch's t test. Bars are ± SEM.

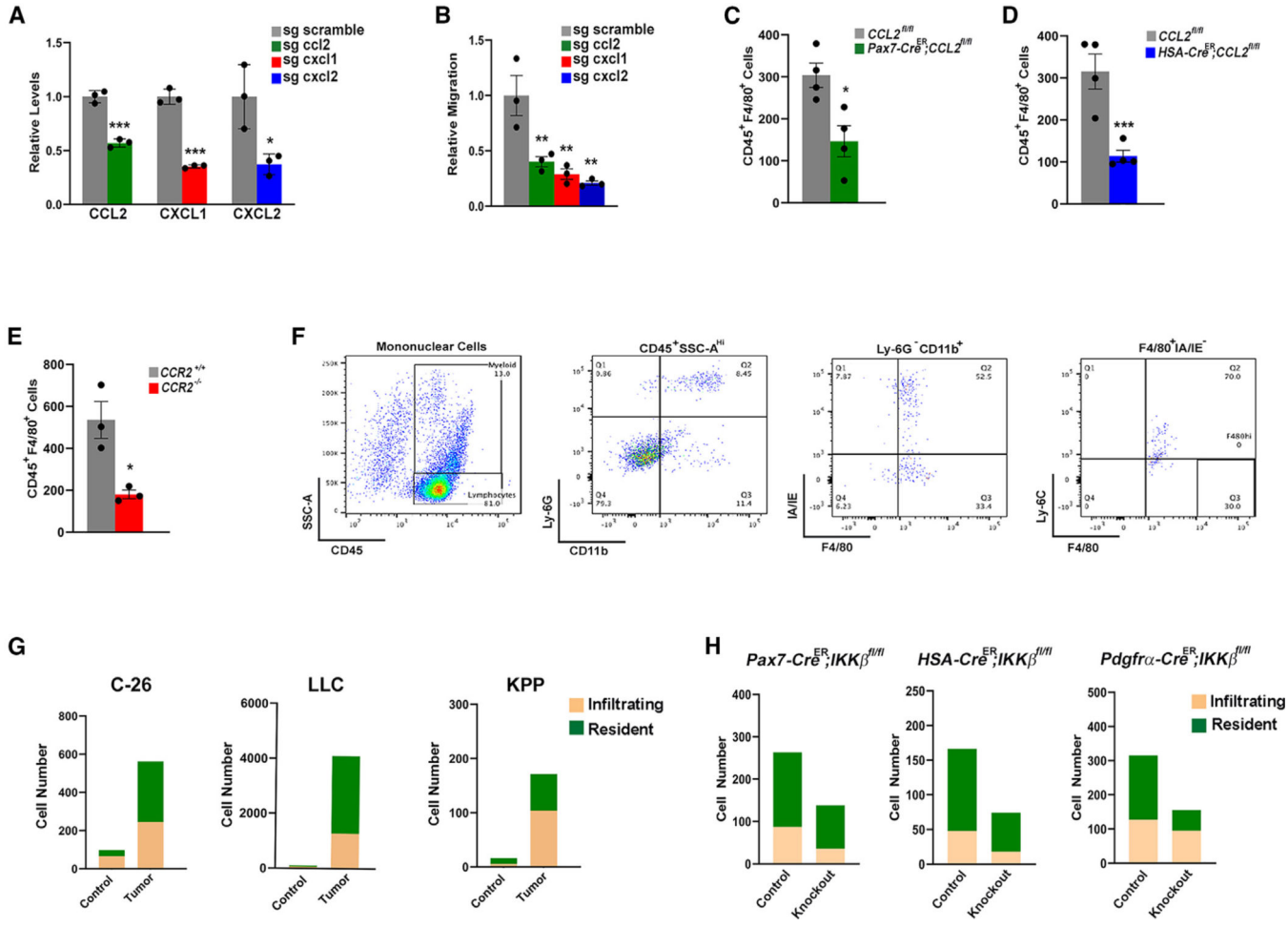

Figure 4. Macrophage accumulation in cachectic muscle derives from both circulating monocytes and resident cells

(A) CCL2, CXCL1, and CXCL2 ELISAs from C2C12 myoblasts containing individual knockdown of CCL2, CXCL1, and CXCL2 chemokines.

(B) Relative migration of RAW264.7 macrophages exposed to conditioned media from C2C12 control (scramble) myoblasts or myoblasts with individual knockdown of chemokines from (A).

(C) Flow cytometry for macrophages in hindlimb muscles of LLC *Pax7-Cre*^{ER}; *CCL2* $^{fl/fl}$.

(D and E) (D) *HSA-Cre*^{ER}; *CCL2* $^{fl/fl}$ and (E) *CCR2*$^{-/-}$ bone marrow-transplanted mice, compared to respective WT controls (*CCL2* $^{fl/fl}$ or *CCR2*$^{+/+}$ bone marrow transplants) (n = 3/genotype).

(F) Flow cytometry plots of resident macrophages from mononuclear cells of C-26 cachectic skeletal muscle.

(G) Representative graphic from flow cytometry of infiltrating (Ly6C^{hi}) and resident (Ly6C^{lo}) macrophages in skeletal muscle from C-26, LLC, and KPP models, compared to control (n = 3/group).

(H) Graphic from flow cytometry of infiltrating (Ly6C^{hi}) and resident (Ly6C^{lo}) macrophages in skeletal muscle from LLC tumor-bearing mice from *Pax7-Cre*^{ER}*; IKKβ* $^{fl/fl}$, *HSA-Cre*^{ER}*; IKKβ* $^{fl/fl}$, and *PDGFRα-Cre*^{ER}*; IKKβ* $^{fl/fl}$ mice, compared to littermate control muscles (n =

3/group); *$p < 0.05$, **$p < 0.01$, and ***$p < 0.001$. Comparisons between two groups were carried out using Student's t test. Bars are ± SEM.

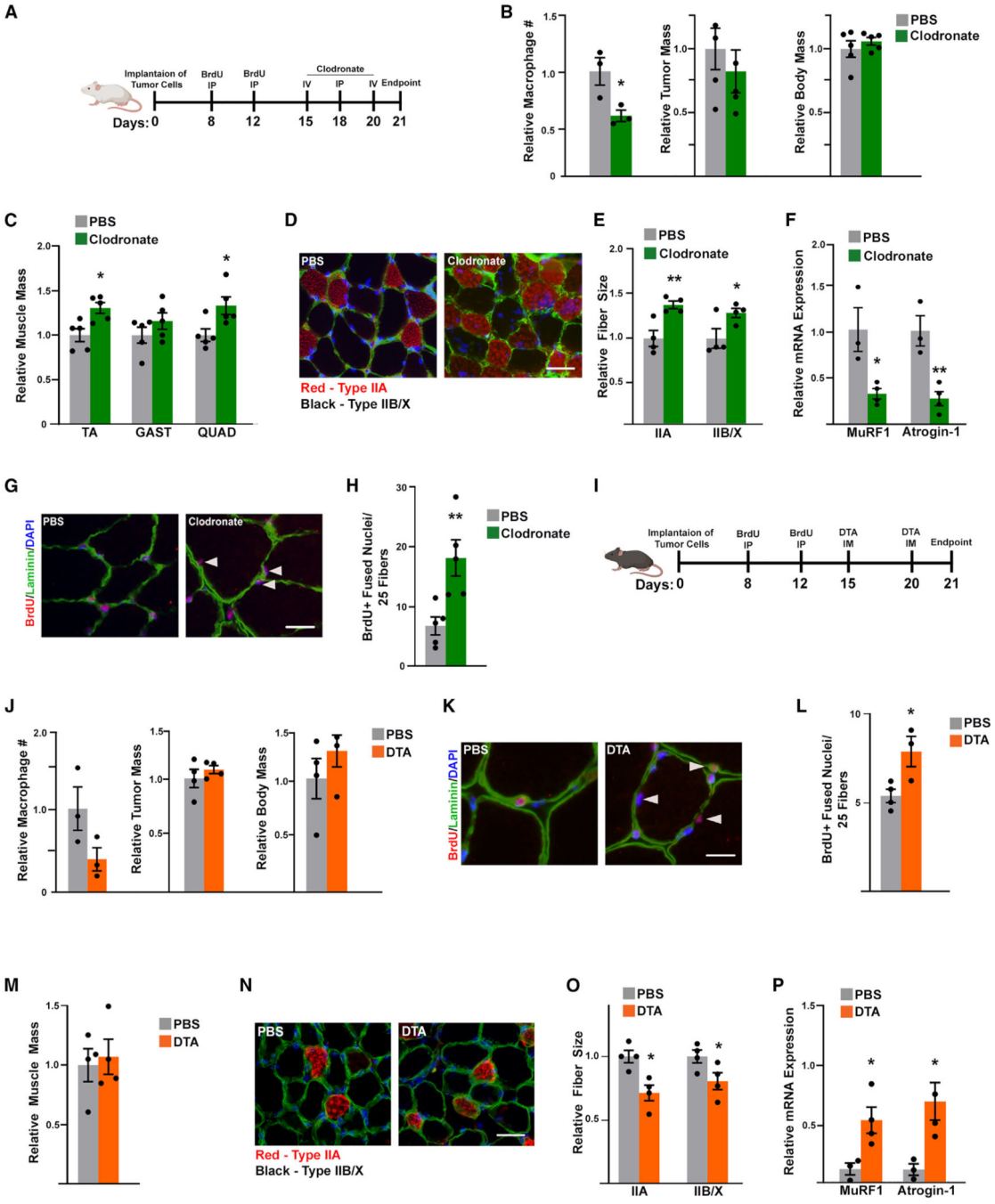

Figure 5. Macrophages exhibit distinct functions in skeletal muscle during cancer cachexia

(A) Design of clodronate treatment of C-26 mice.

(B) Relative number of macrophages quantified by flow cytometry from muscle (n = 3/group), relative tumor mass (n = 5/group), and body mass (n = 5/group) of PBS- or clodronate-treated mice.

(C) Hindlimb muscle mass following administration of PBS or clodronate (n = 5/group) in C-26 tumor-bearing mice.

(D) Immunofluorescence staining with laminin (green) and major histocompatibility complex (MHC) IIA (red) of TA sections from C-26 mice injected with PBS or clodronate. Unstained fibers represent type IIB/X. Scale bar, 50 μm.
(E) Measurements of type IIA and IIB/X fibers obtained from (D) (n = 4/group).
(F) Expression of *MuRF1* and *Atrogin-1* from PBS and clodronate injected mice (n = 3/group).
(G) Immunofluorescence staining of BrdU with laminin in C-26 mice injected with either PBS or clodronate (arrowheads indicate fused sublaminar $BrdU^+$ nuclei). Scale bar, 10 μm.
(H) Measurements of fused $BrdU^+$ nuclei in myofibers obtained from (G) (n = 5/group).
(I) Design for DTA treatment of LLC mice.
(J) Macrophages quantified by flow cytometry from muscle (n = 3/group). Measurements of relative tumor (n = 4/group) and body mass (n = 4/group) in LLC mice following administration of DTA.
(K) Immunofluorescence staining for BrdU with laminin in LLC mice injected with DTA. Scale bar, 10 μm.
(L) Measurements of fused, sublaminar, $BrdU^+$ nuclei in myofibers obtained from (K) (n = 4/group).
(M) Measurements of relative TA muscle mass following DTA treatment in LLC tumor-bearing mice (n = 5/group).
(N) Immunofluorescence staining with laminin (green) and MHC IIA (red) of TA from LLC mice injected with DTA. Unstained fibers represent type IIB/X. Scale bar, 50 μm
(O) Quantitative measurements of type IIA and IIB/X fibers obtained from (N) (n = 4/group).
(P) *MuRF1* and *Atrogin-1* expression in muscles from control or DTA-injected mice (n = 3/group); *$p < 0.05$ and **$p < 0.01$. Comparisons between two groups were carried out using Student's t test. Bars are ± SEM.

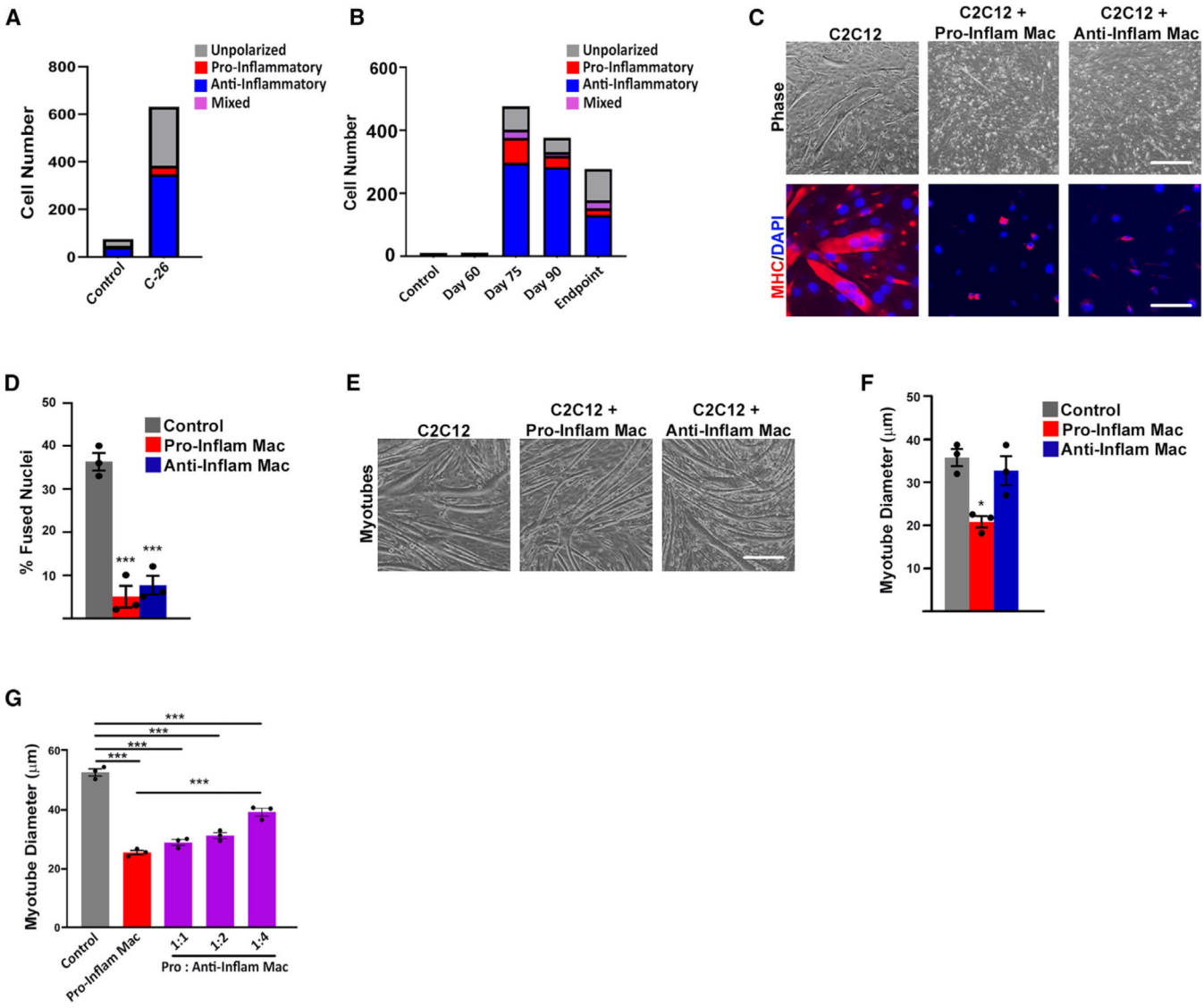

Figure 6. Macrophages polarize to an anti-inflammatory state in cachectic muscle to maintain muscle size while inflammatory macrophages induce muscle atrophy

(A) Flow cytometry of unpolarized ($CD86^{-}/CD206^{-}$), pro-inflammatory ($CD86^{+}$), anti-inflammatory ($CD206^{+}$), and mixed ($CD86^{+}/CD206^{+}$) macrophages in skeletal muscle from control and C-26 mice at endpoint.

(B) Flow cytometry analysis of macrophages, as shown in (A), from KPP muscles at indicated time points.

(C) Phase contrast and immunofluorescence staining for MHC in C2C12 differentiating myoblasts co-cultured with pro-inflammatory or anti-inflammatory macrophages (Mac). Scale bars (upper panel), 100 μm; (lower panel), 30 μm.

(D) Quantification of fused nuclei from (C).

(E) Phase contrast images from C2C12 myotubes co-cultured with pro-inflammatory or anti-inflammatory macrophages (Mac). Scale bar, 100 μm.

(F) Myotube diameter measurements from (E).

(G) Myotube diameter following co-culturing with increasing ratio of anti-to pro-inflammatory macrophages; $^{**}p < 0.01$ and $^{***}p < 0.001$. Multiple group comparisons were carried out using one-way ANOVA followed by Dunnett's or Tukey's multiple comparison test. Bars are ± SEM.

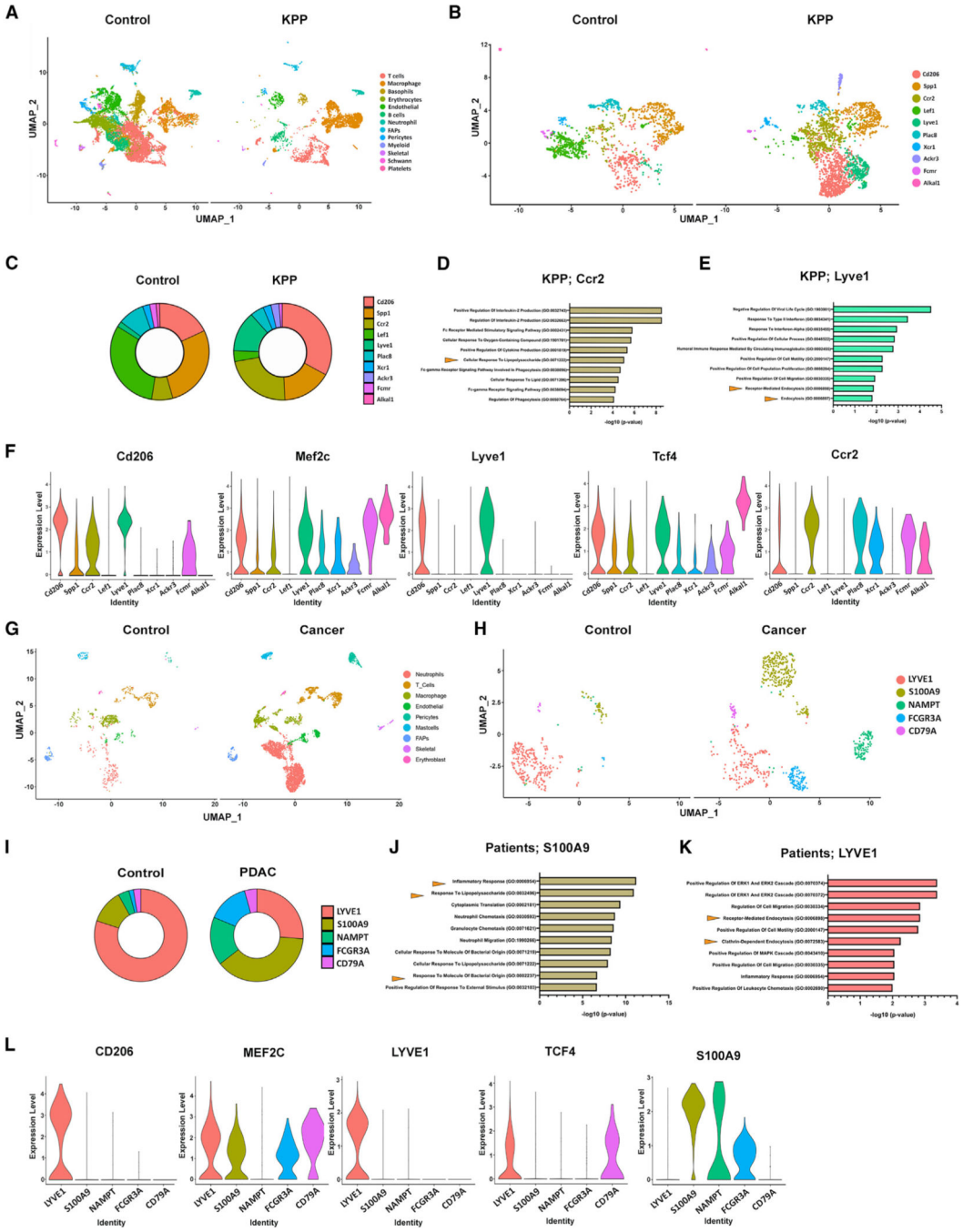

Figure 7. Macrophage subclusters enriched in KPP and cachectic patient muscles

(A) UMAP of CD45^{+} cells isolated from control and KPP muscles.

(B) UMAP of re-clustered macrophage populations from (A) from control and KPP muscles.

(C) Proportion of macrophage subclusters in (B) in control and KPP muscles.

(D and E) GO Biological Processes analysis on Ccr2 (D) and Lyve1 (E) macrophage subclusters from KPP muscles; arrowheads indicate common ontologies.

(F) Violin plots to discriminate between resident, infiltrating, and anti-inflammatory macrophages identified in (B).

(G) UMAP of $CD45^+$ cells isolated from control and PDAC patient muscle.
(H) UMAP of macrophage subclusters from each patient sample in (G).
(I) Proportion of macrophage subclusters in (H) from control and PDAC patient samples.
(J and K) GO Biological Processes analysis on S100A9 (J) and LYVE1 (K) subclusters from control and patients with PDAC; arrowheads indicate common ontologies.
(L) Violin plots for resident macrophage markers in subclusters identified in (H).

KEY RESOURCES TABLE

REAGENT or RESOURCE	SOURCE	IDENTIFIER
Antibodies		
CD11b	Bio X Cell	Cat# BE0007; RRID:AB_1107582
Dystrophin	Santa Cruz	Cat# sc-73592; RRID:AB_1122390
Laminin	abcam	Cat# ab11575; RRID:AB_298179
Pdgfrα (mouse)	R&D	Cat# AF1062; RRID:AB_2236897
Pdgfrα (human)	R&D	Cat# AF-307-NA; RRID:AB_354459
p-p65	Cell Signaling	Cat# 3033; RRID:AB_331284
MYH4	Santa Cruz	Cat# sc-71632; RRID:AB_1126466
BrdU	Abcam	Cat# ab6326; RRID:AB_305426
MF20	DSHB	Cat# MF 20, RRID:AB_2147781
F4/80	Abcam	Cat# ab204266; RRID:AB_2943479)
CD45	Biolegend	Cat# 103138; RRID:AB_2563061
CD206	Biolegend	Cat# 141727; RRID:AB_2565822
CD86	Biolegend	Cat# 105043; RRID:AB_2566722
CD163	Biolegend	Cat# 155305; RRID:AB_2814059
IA/IE	Biolegend	Cat# 107651; RRID:AB_2616728
Siglec F	Thermo Fisher	Cat# 367–1702-80; RRID:AB_2895998
Ly-6C	Biolegend	Cat# 100543; RRID:AB_10898318
CD8a	Biolegend	Cat# 100741; RRID:AB_11124344
CD11b	BD Bioscience	Cat# 564454; RRID:AB_2665392
CD161	Biolegend	Cat# 108745; RRID:AB_2563286
F4/80	Biolegend	Cat# 157303; RRID:AB_2832546
CD3	Biolegend	Cat# 100218; RRID:AB_1595492
CD19	Biolegend	Cat# 115519; RRID:AB_313654
CD25	BD Bioscience	Cat# 561048;RRID:AB_10562035
CD86	Biolegend	Cat# 105045; RRID:AB_2629769
Ly6G	BD Bioscience	Cat# 563978; RRID:AB_2716852
CD45	BD Bioscience	Cat# 740371; RRID:AB_2740103
Donkey anti mouse	Thermo Fisher	Cat# A-31571; RRID:AB_162542
Donkey anti rat	Thermo Fisher	Cat# A-21208; RRID:AB_2535794
Donkey anti rabbit	Thermo Fisher	Cat# A-21206; RRID:AB_2535792
Donkey anti goat	Thermo Fisher	Cat# A-11057; RRID:AB_2534104
Donkey anti rabbit	Thermo Fisher	Cat# A10042; RRID:AB_2534017
Goat anti mouse	Molecular Probes	Cat# A-11031; RRID:AB_144696
Goat anti rat	Thermo Fisher	Cat# A-11077; RRID:AB_2534121
Biotin CD45	Biolegend	Cat# 103103, RRID:AB_312968
Biotin CD31	Biolegend	Cat# 102404, RRID:AB_312899
Biotin Integrin α7	Miltenyi	Cat# 130–128-938; RRID:AB_2905296
PE Ly6A/E	Miltenyi	Cat# 160905; RRID:AB_2910334

REAGENT or RESOURCE	SOURCE	IDENTIFIER
F480	abcam	Cat# ab204266; RRID:AB_2943479
Desmin	abcam	Cat# ab203419; RRID:AB_2943480
CD68	Santa Cruz	Cat# sc-20060; RRID:AB_627158
Biological samples		
rectus abdominal muscle biopsies for single cell sequencing	Medical University of South Carolina	N/A
rectus abdominal muscle biopsies for histology	OSU	N/A
Chemicals, peptides, and recombinant proteins		
tamoxifen	Sigma	T5648–5g
PBS/Clodronate Liposomes	Liposoma	CP-005–005
Diphtheria toxin	Millipore	322326
M-CSF	R&D	416-ML-050/CF
IFNγ	R&D	485-MI-100/CF
IL-4	R&D	404-ML-050/CF
IL-13	R&D	413-ML-050/CF
bFGF	R&D	3139-FB-025/CF
Prolong Gold Antifade DAPI	Invitrogen	P36931
Critical commercial assays		
Mouse CCL2/JE/MCP-1 DuoSet ELISA	R&D	MJE00B
Mouse CXCL1/KC DuoSet ELISA	R&D	DY453
Mouse CXCL2/MIP-2 DuoSet ELISA	R&D	DY452
Human IL-1 beta/IL-1F2 QuicKit ELISA	R&D	QK201
Human IL-6 ELISA Kit - Quantikine	R&D	D6050B
Human TNF-alpha Quantikine QuicKit ELISA	R&D	QK210
Deposited data		
Single Cell data	This paper	GEO: GSE248800
nCounter Inflammation V2 Analysis on Cachectic Mouse Musce	This paper	GEO: GSE245208
RNAseq in Pax7 Cre ErT/IKKβ$^{fl/fl}$ Mice	This paper	GEO: GSE245314
Experimental models: Cell lines		
Colon-26 (C-26)	National Cancer Institute	N/A
Lewis Lung Carcinoma (LLC)	National Cancer Institute	N/A
C2C12	ATCC	CRL-1772
FAPs	This paper	N/A
293T	ATCC	CRL-3216
Experimental models: Organisms/strains		

REAGENT or RESOURCE	SOURCE	IDENTIFIER
Kras $^{LSL-G12D}$	The Jackson Laboratory	RRID:IMSR_JAX:008179
Pten $^{fl/fl}$	The Jackson Laboratory	RRID:IMSR_JAX:006440
Ptf1a $^{Cre-ER}$	The Jackson Laboratory	RRID:IMSR_JAX:019378
CD11b ^{DTR}	The Jackson Laboratory	RRID:IMSR_JAX:006000
CCR2 $^{-/-}$	The Jackson Laboratory	RRID:IMSR_JAX:027619
CCL2 $^{fl/fl}$	The Jackson Laboratory	RRID:IMSR_JAX:016849
IKKβ $^{f/llf}$	The Jackson Laboratory	RRID:MGI:2445462
Pax7 $^{Cre-ER}$	The Jackson Laboratory	RRID:MGI:4436914
HSA $^{Cre-ER}$	The Jackson Laboratory	RRID:IMSR_JAX:025750
Pdgfrα $^{Cre-ER}$	The Jackson Laboratory	RRID:IMSR_JAX:032770
Tnf $^{-/-}$	The Jackson Laboratory	RRID:IMSR_JAX:003008
Il1β $^{-/-}$	The Jackson Laboratory	RRID:IMSR_JAX:034447
B6	Charles River	RRID:IMSR_CRL:027
CD2F1	Charles River	RRID:IMSR_CRL:033
CD45.1	Jackson Lab	RRID:IMSR JAX:002014
Oligonucleotides		
Primers for RT-PCR, see Table S4	This Paper	N/A
Guide RNA sequences, see Table S5	This Paper	N/A
Recombinant DNA		
Lenti sgRNA puro	Addgene	RRID:Addgene_104990
LentiCas9 blast	Addgene	RRID:Addgene_52962
Other		
Single Cell RNA Sequencing Code	This Paper	GitHub - BioinformaticsMUSC/ PryceEtAl_Cachexia: scRNAseq Data Analysis Code